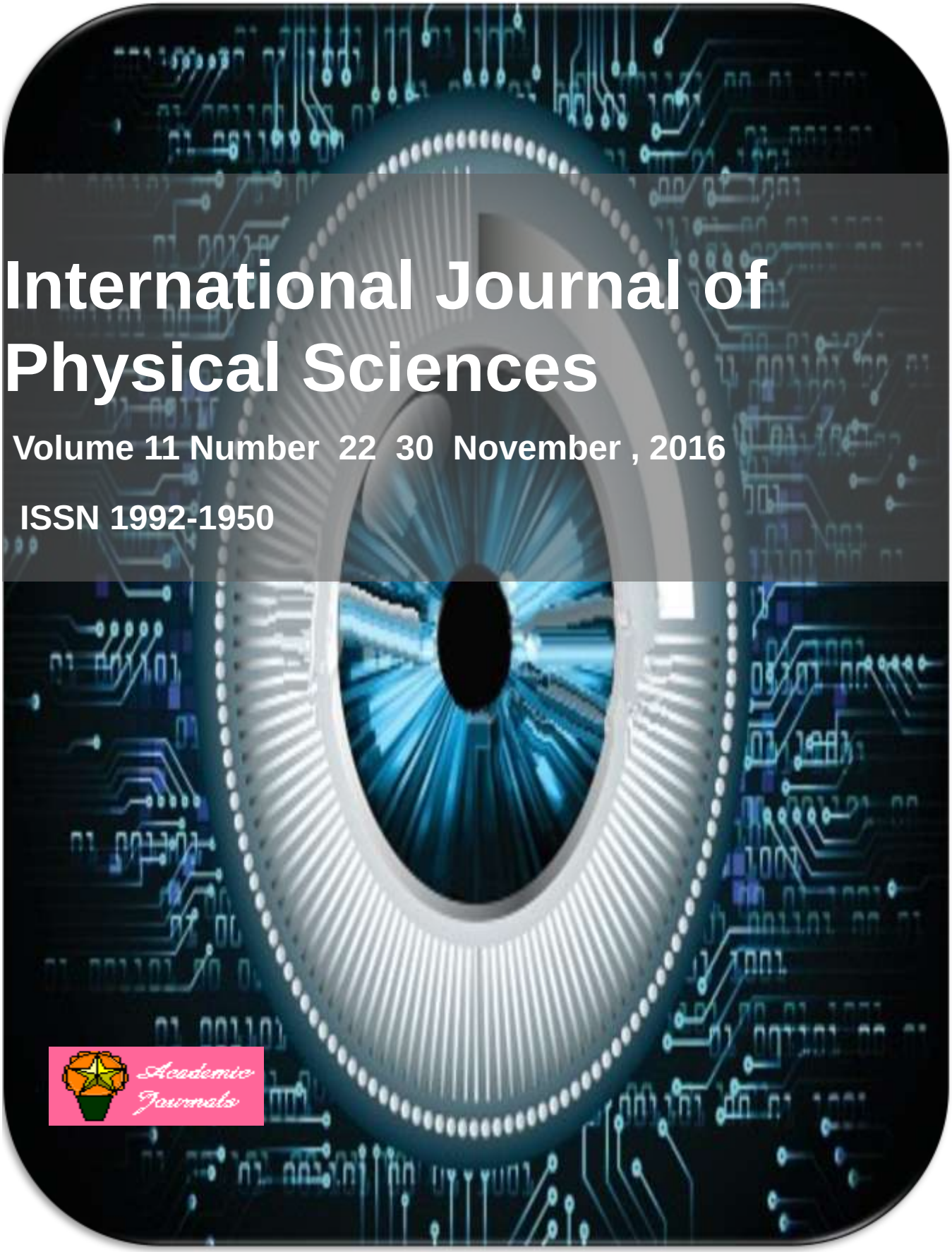

International Journal of Physical Sciences

Volume 11 Number 22 30 November , 2016

ISSN 1992-1950

Academic Journals

ABOUT IJPS

The **International Journal of Physical Sciences (IJPS)** is published weekly (one volume per year) by Academic Journals.

International Journal of Physical Sciences (IJPS) is an open access journal that publishes high-quality solicited and unsolicited articles, in English, in all Physics and chemistry including artificial intelligence, neural processing, nuclear and particle physics, geophysics, physics in medicine and biology, plasma physics, semiconductor science and technology, wireless and optical communications, materials science, energy and fuels, environmental science and technology, combinatorial chemistry, natural products, molecular therapeutics, geochemistry, cement and concrete research, metallurgy, crystallography and computer-aided materials design. All articles published in IJPS are peer-reviewed.

Contact Us

Editorial Office: ijps@academicjournals.org

Help Desk: helpdesk@academicjournals.org

Website: http://www.academicjournals.org/journal/IJPS

Submit manuscript online http://ms.academicjournals.me/

Editorial Board

International Journal of Physical Sciences

Table of Contents: Volume 11 Number 22, 30 November, 2016

ARTICLES

academicJournals

Vol. 11(22), pp. 287-295, 30 November, 2016
DOI: 10.5897/IJPS2016.4503
Article Number: 4A74A9E61631
ISSN 1992 - 1950

http://www.academicjournals.org/IJPS

International Journal of Physical Sciences

Full Length Research Paper

Some fish species in offshore Fukushima, Japan have the ability to accumulate a specific nuclide (radioisotope)

Katsura Hidemitsu[1,2,3]

[1]Coimbatore Institute of Technology (CIT), Coimbatore, Tamil Nadu 641014, India.
[2]Department of Ocean Sciences, Faculty of Marine Science, Tokyo University of Marine Science and Technology, Konan 4-Chome, Minato-Ku, Tokyo 108-8477, Japan.
[3]Institute of Product Design and Manufacturing (IPROM), Universiti Kuala Lumpur (Uni.KL), 119 Jalan 7/91, Taman Shamelin Perkasa, 3.5 Miles Cheras, 56100 Kuala Lumpur, Malaysia.

Received 1 May, 2016; Accepted 30 September, 2016

The Tokyo Electric Power Company's, Fukushima Dai-ichi nuclear power plant in Fukushima-Ken (Fukushima Prefecture), Japan, was destroyed in March 2011 by a massive magnitude 9 earthquake (centred offshore to the northeast of Honshu Island) and by the subsequent historic Tsunami of March 11, 2011. Because of the nuclear meltdown, hydrogen-explosion damage to the buildings that housed the reactors, and the contamination of the cooling water from the reactor cores, large quantities of radioisotopes were emitted into the atmosphere and adjacent seawater. The Tokyo University of Marine Science and Technology has measured radioisotope levels in fishery species off Iwaki-Shi(Iwaki City), Fukushima-Ken (located south of the former nuclear power plant); these data could be used to understand the relationship between the accumulation of specific nuclides (radioisotopes) and certain species of fish, as follows: [1] It is possible to accumulate or separate specific nuclides (134Cs and 137Cs) by combining *Sebastes cheni (Japanese rockfish; SHIROMEBARU)* and *Kareius bicoloratus* (Stone flounder; ISHIGAREI), and *Ditrema temmincki temmincki* (Surfperch; UMITANAGO) and *Cynoglossus joyneri* (Red tongue sole; AKASHITA BIRAME). [2] There are differences in 134Cs and 137Cs accumulation between adult fish and fry of *Paralichthys oli*vaceus (Bastard halibut; HIRAME). Therefore, some fish species have the ability to accumulate a specific nuclide (radioisotope). To date, ultra-centrifugation and diffusion methods have been used to accumulate specific nuclides for atomic fuel. However, if we could use the ability of some fish species to accumulate specific nuclides, we would have additional methods to concentrate nuclides.

Key Words: Nuclide, Accumulate, Fukushima, Fish.

INTRODUCTION

The Tokyo Electric Power Company's, Fukushima Dai-ichi nuclear power plant (37.4212°:N, 141.0334°:E), located in Futaba-Gun (Futaba County), Fukushima-Ken (Fukushima Prefecture), Japan, was destroyed in March

E-mail: hi@katsura.dk Tel: +81-467-54-5869. Fax: +81-467-54-1383.

Table 1. Total fish collection area on 22 to 23 November, 2012.

	Yotsukura	Yotsukura	Ena	Ena (Land Side)	
	Trawl (Net) [Dragneta Trawlnet] (HIKIAMI)	Gill Net (SASHIAMI)	Trawl (Net) [Dragneta Trawlnet] (HIKIAMI) (2 Times)	Gill Net (SASHIAMI)	
Sampling date for weght of fishes	22-Nov-12	22 to 23 NOV-2012	22-Nov-12	22 to 23 NOV-2012	Total Fish Collecting Area in 22 to 23 NOV-2012 [m^2] = [TFCA]
Area [m^2]	9450	28900	9775	50141	98266

2011 by a massive magnitude 9 earthquake (centred offshore to the northeast of Honshu Island) and by the subsequent historic tsunami of March 11, 2011. Because of the resulting nuclear meltdown, the hydrogen-explosion damage to the buildings that housed the reactors, and the contamination of the cooling water from the reactor cores, large quantities of radioisotopes were emitted into the atmosphere and adjacent seawater. From November 22 to 23, 2012, the Tokyo University of Marine Science and Technology independently sampled radioisotope levels in fishery species off Iwaki-Shi (Iwaki City), Fukushima-Ken, just south of the former nuclear power plant. These data included detailed measurements of individual fish such as weight, sex, length, and collection site, which can be used to better understand the accumulation of radioisotopes in fishes. This report shows new insights into the relationship between the accumulation of specific nuclides (radioisotopes) by specific fish species based on this sampling after Katsura's report (Katsura, 2013a; Gerhard et al., 1998; Hellstrom and Brune, 1964; Kalmun, 1982; Murray, 1962; Wolfson, 1956) (Figure 1).

MATERIALS AND METHODS

To sample local fish, trawl (dragnet) fishing was conducted on the November 22, 2012, off Yotsukura and Ena, Iwaki-Shi, Fukushima-Ken, Japan, in a total fishing area of 9,450 and 9,775 m^2, respectively (Atkins and Warren, 1953). Gill-net fishing was conducted from November 22-23, 2012 in the same location, with a total fishing area of 28,900 and 50,141 m^2 off Yotsukura and Ena, respectively (Buscaino et al., 2009). The edible portion of sampled fish was minced and placed into 100 ml plastic containers (U-8 containers). The concentration of Cs-134 and Cs-137 radioisotopes in the fish biomass were measured by IDEA Consultants Inc. (Tokyo, Japan) using a germanium semiconductor detector (Seiko EG&G Co.Model:GEM20-70) (Inazu et al., 2011; Minatani et al., 2012).

RESULTS AND DISCUSSION

The total fish-collection area for November 22-23, 2012 as shown in Table 1 was calculated as follows (Katsura, 2013b):

9,450+28,900+9,775+50,141= 98,266 m^2

Table 2 shows the following:

i) [Percentage of Total Fish Weight] = [%TFW] is the percentage that each species of fish has with respect to the total fish weight sampled.

ii) ([134Cs per Fish Species] / [Total 134Cs for All Species]) × 100

= ([134Cs] / [T134Cs]) × 100=[134Cs%]

is the percentage of 134Cs becquerel that each fish species has of the total 134Cs becquerel for all fish species (Bq is the symbol for "becquerel", an SI derived unit of radioactivity; One Bq is defined as the activity of a quantity of radioactive material in which one nucleus decays per second) (Choppin et al., 2002).

iii) ([137Cs per Fish Species]/[Total 137Cs All Species]) x 100 =([137Cs]/[T137Cs])x100=[137Cs%]

is the percentage of 137Cs becquerel that each fish species has of the total 137Cs becquerel for all fish species sampled.

iv) Tables 3 and 4 show the proportion of 134Cs and 137Cs accumulated by each fish species according to their percentage of the total fish weight in descending order, as follows:

[134Cs%]/[%TFW] × 100

[137Cs%]/[%TFW] × 100

If there was a proportional relationship between the amount of 134Cs or 137Cs Bq (that is, quantity of 134Cs or 137Cs radioactive material) in sampled fish body weight regardless of species, all percentages of 134Cs or 137Cs Bq per percentage of total fish weight should be 100% (Table 5).

Table 2. Amount of fishery resources and the total amount of cesium radioisotopes in fish bodies in offshore Fukushima-Ken, Japan in Nov. 2012.

Scientific name	Japanese Name	Weight [g]	Weight %	Weight [g]	Weight %	Weight [g]	Weight %	Weight [g]	Weight %	Weight [g]	Weight %	Each species of total fish weight [g]	[%TFW]	[134Cs]	[134Cs%]	[137Cs]	[137Cs%]
		Yotsukura				Ena		Ena (Land Side)		Ena (Offshore Side)							
		By Trawl (Net)		By Gill Net		By Trawl (Net) (2 times)		By Gill Net		By Gill Net							
Acanthopagrus schlegeli	Kurodai	2000	1.456261195	0	0	0	0	0	0	0	0	2000	0.743555235	0	0	0	0
Chelidonichthys spinosus	Houbou	0	0	1170	3.549757282	0	0	0	0	0	0	1170	0.434979812	7.015	0.057003374	10.085	0.047709706
Clupea pallasii Vakenciennes	Nishin	23	0.016747004	0	0	0	0	0	0	0	0	23	0.008550885	0	0	0	0
Cynoglossus joyneri	Akashita Birame	600	0.436878359	0	0	1810	4.815110402	300	2.284843869	0	0	2710	1.007517343	14.1	0.265384423	22.25	0.243805938
Ditrema temminkii	Umi Tanago	0	0	0	0	0	0	210	1.599390708	2960	6.171809842	3170	1.178535047	12.445	0.273994086	22.3	0.285830849
Engraulis japonica	Katakuchi Iwashi	88	0.064075493	0	0	0	0	0	0	0	0	88	0.03271643	0	0	0	0
Hexagrammos otakii	Ainame	0	0	2130	6.462378641	0	0	1060	8.073115004	1810	3.773978315	5000	1.858888088	52.19230769	1.812439544	88.01538462	1.779399929
Hexagrammos stelleri	Ezo Iso Ainame	0	0	0	0	0	0	330	2.513328256	940	1.959966639	1270	0.472157574	21.9	0.193167857	37.36666667	0.191881477
Kareius bicoloratus	Ishi Garei	0	0	750	2.275485437	920	2.447459431	0	0	0	0	1670	0.620868621	130	1.507810796	213	1.438272074
Lateolabrax japonicus	Suzuki	0	0	0	0	1300	3.458366587	0	0	0	0	1300	0.483310903	53.9	0.486652706	98.6	0.518280944
Lepidotrigla microptena Gunther	Kana Gashira	280	0.203876567	0	0	0	0	0	0	0	0	280	0.104097733	0	0	0	0
Liparis tanakai	Kusauo	310	0.225720485	0	0	0	0	0	0	0	0	310	0.115251061	0	0	0	0
Mlicrostomus achn	Baba Garei	0	0	2600	7.888349515	0	0	0	0	850	1.772310259	3450	1.28263278	107.8333333	2.583801526	187.3333333	2.61323899
Mustelus manazo	Hoshi Zame	50500	36.77059517	0	0	11100	29.52913009	0	0	0	0	61600	22.90150124	0	0	0	0
Nibea mitsukurii	Nibe	0	0	0	0		0	1140	8.682406702	1040	2.168473728	2180	0.810475206	16.66	0.252242647	29.9	0.263555847
Okamejei kenojei	Komon Kasube (Tsumari Kasube)	56900	41.430631	1390	4.21723301	13480	35.86060122	0	0	0	0	71770	26.68247961	98.95	49.32257817	173.95	50.47918713
Oncorhynchus keta	Sake	0	0	0	0	0	0	0	0	500	1.042535446	500	0.185888809	0	0	0	0
Oplegnathus punctatus	Ishigaki Dai	0	0	640	1.941747573	0	0	0	0	0	0	640	0.237937675	0	0	0	0
Pagrus major	Madai	0	0	0	0	0	0	0	0	290	0.604670559	290	0.107815509	0	0	0	0
Pagrus major (Fry)	Madai (Chigyo)	322	0.234458052	0	0	0	0	0	0	0	0	322	0.119712393	0	0	0	0
Paralichthys olivaceus	Hirame	1600	1.165008956	6280	19.05339806	5340	14.20590583	0	0	2500	5.212677231	15720	5.844344147	14.98	1.635503132	25.74727273	1.636548003
Paralichthys olivaceus (Fry)	Hirame (Chigyo)	34	0.02475644	0	0	0	0	0	0	0	0	34	0.012640439	0	0	0	0
Platycephalus sp.2	Magochi	580	0.422315747	0	0	450	1.197126895	0	0	0	0	1030	0.382930946	0	0	0	0
Platycephalus sp.2 (fry)	Magochi (Chigyo)	10	0.007281306	0	0	0	0	0	0	0	0	10	0.003717776	0	0	0	0
Scyliorhinus torazame	Tora Zame	5200	3.786279107	250	0.758495146	3190	8.486299548	0	0	0	0	8640	3.212158615	27.00583333	1.620534759	47.58	1.662199524
Sebastes cheni	Shiro Mebaru	0	0	200	0.606796117	0	0	8890	67.70753998	27760	57.88156797	36850	13.7000052	129.0857143	33.03715945	213.2857143	31.77929316
Sebastes inermis	Aka Mebaru	0	0	0	0	0	0	0	0	1020	2.12677231	1020	0.37921317	96.175	0.681317261	160.15	0.660498884
Sebastes pachycephalus pachycephalus	Murasoi	0	0	0	0	0	0	330	2.513328256	1760	3.669724771	2090	0.777015221	40.175	0.583161973	70.65	0.597039996
Sebastes vulpes	Kitsune Mebaru	0	0	1260	3.822815534	0	0	590	4.493526276	6530	13.61551293	8380	3.115496435	32.4	1.885714992	59.068	2.001433931
Sebastiscus marmoratus	Kasago	0	0	0	0	0	0	280	2.132520944	0	0	280	0.104097733	38.3	0.074480714	67.1	0.075967096
Seriola quinqueradiata	Buri	0	0	1670	5.066747573	0	0	0	0	0	0	1670	0.620868621	4.03	0.046742135	5.09	0.034369976
Takifugu poecilonotus	Komon Fugu	70	0.050969142	0	0	0	0	0	0	0	0	70	0.026024433	0	0	0	0
Takifugu rubipes	Tora Fugu	1610	1.172290262	0	0	0	0	0	0	0	0	1610	0.598561964	83.9	0.938155571	135	0.878829483
Takifugu snyderi	Shousai Fugu	16200	11.79571568	0	0	0	0	0	0	0	0	16200	6.022797404	0	0	0	0
Takifugu stictonotus	Goma Fugu	120	0.087375672	0	0	0	0	0	0	0	0	120	0.044613314	0	0	0	0
Trachurus japonicus	Ma Aji	887	0.64585184	0	0	0	0	0	0	0	0	887	0.329766747	0	0	0	0

Table 2. Contd.

Triakis scyllium	Dochi Zame	0	0	14620	44.35679612	0	0	0	0	0	0	14620	5.435388768	27.00583333	2.742154881	47.58	2.812657065
Zeus faber Linnaeus	Matou Dai	4	0.002912522	0	0	0	0	0	0	0	0	4	0.00148711	0	0	0	0
	Total Fish Weight	137338	100	32960	100	37590	100	13130	100	47960	100	268978					

The percentage that each species of fish has with respect to the total fish sampled = [%TFW]; (134Cs per Fish Species) [becquerel]/[kg] = [134Cs]; ([134Cs per Fish Species]/[Total 134Cs for All Species])x100 [%] = [134Cs%]; (137Cs per Fish Species) [becquerel]/[kg] = [137Cs]; ([137Cs per Fish Species]/[Total 134Cs for All Species])x100 [%] = [137Cs%].

However, these percentages vary depending on fish species from 0 to 242.855% for 134Cs and from 0 to 231.9655554% for 137Cs.

The values of

[134Cs%] / [%TFW] × 100

and

[137Cs%] / [%TFW] × 100

for the following species are 0%: *Acanthopagrus schlegeli* (Japanese black seabream; KURODAI), *Clupea pallasii Vakenciennes* (Pacific herring; NISHIN), *Engraulis japonica* (Japanese anchovy; KATAKUCHI IWASHI), *Lepidotrigla microptena Gunther* (Gurnard, Sea-robin; KANAGASHIRA), *Liparis tanakai* (English Name: Not-Available=N/A; KUSAUO), *Mustelus manazo* (Starspotted smooth hound; HOSHI-ZAME), *Oncorhynchus keta* (Chum salmon, Salmon; SAKE), *Oplegnathus punctatus* (Spotted Knifejaw; ISHIGAKIDAI), *Pagrus major* (Red seabream; MADAI (SEIGYO)), *P. major (fry)* (Redseabream (Fry); MADAI (CHIGYO)), *Paralichthys olivaceus (fry)* (Bastard halibut (Fry); HIRAME (CHIGYO)), *Platycephalus sp.* (Flathead; MAGOCHI), *Platycephalus sp. (fry)* (Flathead (Fry); MAGOCHI (CHIGYO)), *Takifugu poecilonotus* (Pufferfish; Name: KOMON FUGU), *Takifugu snyderi* (Globefish, Blowfish, Puffer; SHOUSAI FUGU), *Takifugu stictonotus* (Globefish, Blowfish, Puffer; GOMA FUGU), *Trachurus japonicas* (Japanese jack mackerel. Japanese horse mackerel, Japanese scad; MAAJI) and *Zeus faber Linnaeus* (John dory; MATOU DAI). These findings indicate that these fish species do not have the ability to accumulate 134Cs and 137Cs radioisotopes. In other words, these species eliminate 134Cs and 137Cs radioisotopes from their bodies.

iv) Tables 3 and 4 show the differences in the 134Cs and 137Cs accumulation ratio depending on fish species; some species accumulate more 134Cs whereas other species accumulate more 137Cs.

Thus, the order values of

([134Cs%] / [%TFW]) × 100% and ([137Cs%] / [%TFW]) × 100%

are reversed. In detail, it has the following features.

a) The order value of

([137Cs%] / [%TFW]) × 100%

of *Sebastes cheni* (Japanese rockfish, Japanese sea perch; SHIRO MEBARU) is higher than that of *Kareius bicoloratus* (Stone flounder; ISHIGAREI). However, the order value of ([134Cs%] / [%TFW]) × 100% of *Kareius bicoloratus* is higher than that of *Sebastes cheni*. Therefore, it may be possible to use *Sebastes cheni* and *Kareius bicoloratus* for the separation or accumulation of nuclide 134CS and 137Cs. *Sebastes cheni* shows

((231.965554-231.6548179) / 231.6548179) × 100=0.13413755 Weight%

higher accumulation than *Kareius bicoloratus* for 137Cs.

However, *Kareius bicoloratus* shows

((242.85505-241.14706) / 241.14706) × 100=0.708277347 Weight%

higher accumulation than *Sebastes cheni* for 134Cs.

Therefore, it may be possible to use *Sebastes cheni* and *Kareius bicoloratus* for the accumulation or separation for specific nuclides 134Cs and 137Cs.

b) The order value of

([137Cs%] / [%TFW]) × 100%

of *Ditrema temminkii* (Surfperch; Japanese Name: UMITANAGO) is higher than that of *Cynoglossus joyneri* (Red tongue sole; AKASHITA BIRAME) (Figure 4) and the order value of:

Table 3. The order value of ([134Cs%]/[%TFW])x100%.

Number (Order value of the right is less)	([134Cs%]/[%TFW%]) x100 [%]	Scientific Name	Species Japanese Name
1	0	*Acanthopagrus schlegeli*	Kurodai
2	0	*Clupea pallasii Vakenciennes*	Nishin
3	0	*Engraulis japonica*	Katakuchi Iwashi
4	0	*Lepidotrigla microptena Gunther*	Kana Gashira
5	0	*Liparis tanakai*	Kusauo
6	0	*Mustelus manazo*	Hoshi Zame
7	0	*Oncorhynchus keta*	Sake
8	0	*Oplegnathus punctatus*	Ishigaki Dai
9	0	*Pagrus major*	Madai
10	0	*Pagrus major (Fry)*	Madai (Chigyo)
11	0	*Paralichthys olivaceus (Fry)*	Hirame (Chigyo)
12	0	*Platycephalus sp.2*	Magochi
13	0	*Platycephalus sp.2 (fry)*	Magochi (Chigyo)
14	0	*Takifugu poecilonotus*	Komon Fugu
15	0	*Takifugu snyderi*	Shousai Fugu
16	0	*Takifugu stictonotus*	Goma Fugu
17	0	*Trachurus japonicus*	Ma Aji
18	0	*Zeus faber Linnaeus*	Matou Dai
19	7.5285065	*Seriola quinqueradiata*	Buri
20	13.104832	*Chelidonichthys spinosus*	Houbou
21	23.248701	*Ditrema temminkii*	Umi Tanago
22	26.340432	*Cynoglossus joyneri*	Akashita Birame
23	27.984374	*Paralichthys olivaceus*	Hirame
24	31.122809	*Nibea mitsukurii*	Nibe
25	40.911735	*Hexagrammos stelleri*	Ezo Iso Ainame
26	50.450023	*Scyliorhinus torazame*	Tora Zame
27	50.450023	*Triakis scyllium*	Dochi Zame
28	60.526951	*Sebastes vulpes*	Kitsune Mebaru
29	71.548834	*Sebastiscus marmoratus*	Kasago
30	75.051551	*Sebastes pachycephalus pachycephalus*	Murasoi
31	97.501273	*Hexagrammos otakii*	Ainame
32	100.69144	*Lateolabrax japonicus*	Suzuki
33	156.73491	*Takifugu rubipes*	Tora Fugu
34	179.66603	*Sebastes inermis*	Aka Mebaru
35	184.85005	*Okamejei kenojei*	Komon Kasube
36	201.44515	*Mlicrostomus achn*	Baba Garei
37	241.14706	*Sebastes cheni*	Shiro Mebaru
38	242.85505	*Kareius bicoloratus*	Ishi Garei

([134Cs%] / [%TFW]) x 100%

of *Cynoglossus joyneri* is higher than that of *Ditrema temminkii.* Therefore, it may be possible to use *Ditrema temminkii* and *Cynoglossus joyneri* for the separation or accumulation of nuclide 134CS and 137Cs. *Ditrema temminkii* shows

((24.2530309-24.19868403) / 24.19868403) × 100=0.224719079 Weight%

higher accumulation than *Cynoglossus joyneri* for 137Cs. However, *Cynoglossus joyneri* shows

((26.340432-23.248701) / 23.278701) × 100=13.29851074 Weight%

higher accumulation than *Ditrema temminkii* for 134Cs. Therefore, it may be possible to use *Ditrema temminkii* and *Cynoglossus joyneri* for the accumulation or

Table 4. The order value of ([137Cs%]/[%TFW])x100%.

Number (Order value of the right is less)	([137Cs%]/[%TFW%]) x 100 [%]	Scientific Name	Species Japanese Name
1	0	*Acanthopagrus schlegeli*	Kurodai
2	0	*Clupea pallasii Vakenciennes*	Nishin
3	0	*Engraulis japonica*	Katakuchi Iwashi
4	0	*Lepidotrigla microptena* Gunther	Kana Gashira
5	0	*Liparis tanakai*	Kusauo
6	0	*Mustelus manazo*	Hoshi Zame
7	0	*Oncorhynchus keta*	Sake
8	0	*Oplegnathus punctatus*	Ishigaki Dai
9	0	*Pagrus major*	Madai
10	0	*Pagrus major (Fry)*	Madai (Chigyo)
11	0	*Paralichthys olivaceus (Fry)*	Hirame (Chigyo)
12	0	*Platycephalus sp.2*	Magochi
13	0	*Platycephalus sp.2 (fry)*	Makochi (Chigyo)
14	0	*Takifugu poecilonotus*	Komon Fugu
15	0	*Takifugu snyderi*	Shousai Fugu
16	0	*Takifugu stictonotus*	Goma Fugu
17	0	*Trachurus japonicus*	Ma Aji
18	0	*Zeus faber Linnaeus*	Matou Dai
19	5.53578884	*Seriola quinqueradiata*	Buri
20	10.96825746	*Chelidonichthys spinosus*	Houbou
21	24.19868403	*Cynoglossus joyneri*	Akashita Birame
22	24.25306309	*Ditrema temminkii*	Umi Tanago
23	28.00225246	*Paralichthys olivaceus*	Hirame
24	32.51868101	*Nibea mitsukurii*	Nibe
25	40.63928808	*Hexagrammos stelleri*	Ezo Iso Ainame
26	51.74711847	*Triakis scyllium*	Dochi Zame
27	51.74711847	*Scyliorhinus torazame*	Tora Zame
28	64.2412525	*Sebastes vulpes*	Kitsune Mebaru
29	72.97670554	*Sebastiscus marmoratus*	Kasago
30	76.83761917	*Sebastes pachycephalus pachycephalus*	Murasoi
31	95.72388683	*Hexagrammos otakii*	Ainame
32	107.2355166	*Lateolabrax japonicus*	Suzuki
33	146.8234761	*Takifugu rubipes*	Tora Fugu
34	174.1761459	*Sebastes inermis*	Aka Mebaru
35	189.1847679	*Okamejei kenojei*	Komon Kasube
36	203.7402311	*Mlicrostomus achn*	Baba Garei
37	231.6548179	*Kareius bicoloratus*	Ishi Garei
38	231.9655554	*Sebastes cheni*	Shiro Mebaru

separation of specific nuclides 134Cs and 137Cs.

v) Additionally, Tables 3 and 4 show accumulation ratio differences between adult fish and fry of the same species.

a) *Pagrus major* (Adult Fish) (Red seabream (Adult Fish); MADAI (SEIGYO)), *Pagrus major* (Fry) (Red seabream (Fry); MADAI (CHIGYO)), *Platycephalus* sp. (Adult Fish) (Flathead (Adult Fish); MAGOCHI (SEIGYO)) and *Platycephalus* sp.(fry) (Flathead (Fry); MAGOCHI (CHIGYO)) do not have the ability to accumulate both 134Cs and 137Cs. Additionally, there do not appear to be any differences between adult fish and fry for the accumulation 134Cs and 137Cs.

b) *Paralichthys olivaceus* (Adult Fish) (Bastard halibut (Adult Fish); HIRAME (SEIGYO)) has the ability to accumulate both134Cs and 137Cs; however, *Paralichthys*

Table 5. Total grand fish weight % [%TFW].

Number (Order value of the right is less)	Total Fish Weight %=[%TFW]	Scientific Name	Species Japanese Name
1	0.0014871	*Zeus faber* Linnaeus	Matou Dai
2	0.0037178	*Platycephalus sp.2 (fry)*	Makochi (Chigyo)
3	0.0085509	*Clupea pallasii Vakenciennes*	Nishin
4	0.0126404	*Paralichthys olivaceus (Fry)*	Hirame (Chigyo)
5	0.0260244	*Takifugu poecilonotus*	Komon Fugu
6	0.0327164	*Engraulis japonica*	Katakuchi Iwashi
7	0.0446133	*Takifugu stictonotus*	Goma Fugu
8	0.1040977	*Lepidotrigla microptena* Gunther	Kana Gashira
9	0.1040977	*Sebastiscus marmoratus*	Kasago
10	0.1078155	*Pagrus major*	Madai
11	0.1152511	*Liparis tanakai*	Kusauo
12	0.1197124	*Pagrus major (Fry)*	Madai (Chigyo)
13	0.1858888	*Oncorhynchus keta*	Sake
14	0.2379377	*Oplegnathus punctatus*	Ishigaki Dai
15	0.3297667	*Trachurus japonicus*	Ma Aji
16	0.3792132	*Sebastes inermis*	Aka Mebaru
17	0.3829309	*Platycephalus sp.2*	Magochi
18	0.4349798	*Chelidonichthys spinosus*	Houbou
19	0.4721576	*Hexagrammos stelleri*	Ezo Iso Ainame
20	0.4833109	*Lateolabrax japonicus*	Suzuki
21	0.598562	*Takifugu rubipes*	Tora Fugu
22	0.6208686	*Kareius bicoloratus*	Ishi Garei
23	0.6208686	*Seriola quinqueradiata*	Buri
24	0.7435552	*Acanthopagrus schlegeli*	Kurodai
25	0.7770152	*Sebastes pachycephalus pachycephalus*	Murasoi
26	0.8104752	*Nibea mitsukurii*	Nibe
27	1.0075173	*Cynoglossus joyneri*	Akashita Birame
28	1.178535	*Ditrema temminkii*	Umi Tanago
29	1.2826328	*Mlicrostomus achn*	Baba Garei
30	1.8588881	*Hexagrammos otakii*	Ainame
31	3.1154964	*Sebastes vulpes*	Kitsune Mebaru
32	3.2121586	*Scyliorhinus torazame*	Tora Zame
33	5.4353888	*Triakis scyllium*	Dochi Zame
34	5.8443441	*Paralichthys olivaceus*	Hirame
35	6.0227974	*Takifugu snyderi*	Shousai Fugu
36	13.700005	*Sebastes cheni*	Shiro Mebaru
37	22.901501	*Mustelus manazo*	Hoshi Zame
38	26.68248	*Okamejei kenojei*	Komon Kasube

Each species of fish has how much weight percent of total fish weight in this sampling in offshore Fukushima-ken, Japan in November 2012.

olivaceus (Fry) (Bastard halibut (Fry); HIRAME (CHIGYO)) does not have ability to accumulate both 134Cs and 137Cs. There are differences between adult fish and fry of *Paralichthys olivaceus* for the accumulation of 134Cs and 137Cs.

vi) It is currently known that specific fish species have the ability to accumulate specific elements, ions and molecules (Thompson et al., 1972). However, the accumulation of specific radioisotopes had not been reported until this and Katsura's research article (Katsura, 2013a). The disaster at Fukushima on March 11, 2011 provides the opportunity to gain new insight into the accumulation of specific radioisotopes by fishes. We must discover the theoretical reasons for these phenomena in order to use fishes as new methods for atomic fuel production and clean-up of specific radioisotope contamination.

Figure 1. Okamejei konojei.

Figure 2. *Sebastes cheni*.

Conclusion

1) This finding indicates that the following fishes do not have the ability to accumulate the 134Cs and 137Cs radioisotopes: *Acanthopagrus schlegeli* (Japanese black seabream; KURODAI), *Clupea pallasii Vakenciennes* (Pacific herring; NISHIN), *Engraulis japonica* (Japanese anchovy; KATAKUCHI IWASHI), *Lepidotrigla microptena Gunther* (Gurnard, Sea-robin; KANAGASHIRA), *Liparis tanakai* (English Name: Not Available=N/A; KUSAUO), *Mustelus manazo* (Starspotted smooth hound; HOSHIZAME), *Oncorhynchus keta* (Chum salmon, Salmon; SAKE), *Oplegnathus punctatus* (Spotted Knifejaw; ISHIGAKI DAI), *Pagrus major* (Red seabream; MADAI), *Pagrus major (Fry)* (Red seabream (Fry); MADAI (CHIGYO)), *Paralichthys olivaceus (Fry)* (Bastard halibut (Fry); HIRAME (CHIGYO)), *Platycephalus sp.* (Flathead; MAGOCHI), *Platycephalus sp. (fry)* (Flathead (Fry); MAGOCHI (CHIGYO)), *Takifugu poecilonotus* (Pufferfish; KOMON-FUGU), *Takifugu snyderi* (Globefish, Blowfish, Puffer; SHOUSAI-FUGU), *Takifugu stictonotus* (Globefish, Blowfish, Puffer; GOMA-FUGU), *Trachurus-japonicas* (Japanese jack mackerel. Japanese horse mackerel, Japanese scad; MAAJI) and *Zeus faber* Linnaeus (John-dory; MATOUDAI). Several fish species are able to eliminate 134Cs and 137Cs radioisotopes.

2) It is possible to accumulate or separate specific radioisotopes (134Cs or 137Cs) by combining the following fish species: *Sebastes cheni* (Japanese rockfish, Japanese sea perch; SHIRO-MEBARU) (Figure 2) and *Kareius bicoloratus* (Stone flounder; ISHIGAREI) (Figure 3); and *Ditrema temminkii* (Surfperch; UMITANAGO) (Figure 5) and *Cynoglossus joyneri* (Red tongue sole; AKASHITA BIRAME) (Figure 4).

3) Neither *Pagrus major* (Red seabream; MADAI) nor *Platycephalus* sp. (Flathead; MAGOCHI) adult fish and fry accumulated 134Cs and 137Cs. There were differences in the accumulation of 134Cs and 137Cs between adult fish and fry of *Paralichthys olivaceus* (Bastard halibut; HIRAME).

Figure 3. *Kareius bicoloratus.*

Figure 4. *Cynoglossus jpyneri*

Figure 5. *Ditrema temminkii.*

4) Physical methods such as ultra-centrifugation and diffusion have been used to obtain high concentrations of nuclides (e.g., 235 U). This study suggests that physical methods are not required to accumulate high concentrations of specific radioisotopes.

Conflict of interests

The author has not declared any conflict of interest.

ACKNOWLEDGEMENTS

The author is grateful to Ms. Harriet Kim Anh Rodis, Graphic Artist in Angeles City, Philippines; Dr. Darulihsan Abdul Hamid, Associated Professor, Program Director for MJHEP, Institute of Product Design and Manufacturing (IPROM), Universiti Kuala Lumpur (UniKL); Dr. Adnan Bin Ibrahim, Associated Professor, Deputy Dean, IPROM, UniKL; Dr. Mohd Razif Idris, Associated Professor, Dean, IPROM, UniKL; Dr. Ahmad Zakaria, Professor, IPROM, UniKL; Ms. Ariki Mizuki, Ms. Gorai Myu, Ms. Henmi Chikako, Mr. Kase Ryota, Mr. Nakagawa Takuro and Mr. Myouse Hiroshi, undergraduate students at the Tokyo University of Marine Science and Technology (TUMST); Ms. Shimomura Yukiko, Mr. Hasegawa Kouhei, and Mr. Watanabe Hayato, graduate students at TUMST; Ph.D. Candidate Girault Mathias and Ph.D. Candidate Matsumoto Akira at TUMST; Mr. Sato Katsuhiro and Ms. Yoshizaki Kae, Research Scientists, TUMST; Ms. Honda Tomoko, Secretary to Professor Arakawa Hisayuki, TUMST; Dr. Wakabayashi Kaori, Doctoral Research Scientist, TUMST; Dr. Norman Chris, Adjunct Professor, TUMST; Dr. Akiyama Seiji, Assistant Professor, TUMST; Dr. Uchida Keiichi, Assistant Professor, TUMST; Dr. Arakawa Hisayuki, Professor, TUMST and Dr. Morinaga Tsutomu, Emeritus Professor TUMST and Ms. Katsura Sakie, Former Director General of the Nursing Department at Saiseikai Kanagawa-Ken Hospital by the Social Welfare Organization Saiseikai Imperial Gift Foundation Inc. in Japan for assisting with this study. This study was supported by the Research Trust Fund for fiscal year 2012 of the Ministry of the Environment, Japan for “Study of the diffusion process of radioisotope materials from the destroyed nuclear power plant in offshore ecosystems in Fukushima-Ken, Japan [HEISEI24NENDO KANKYOUSHOU SOUGOU KENKYUU SUISHINHI]”.

REFERENCES

Atkins WRG, Warren FJ (1953). The preservation of fishing nets, trawl twines, and fiber ropes for use in sea water. J. Mar. Biol. Assoc. UK. 31:509-513.

Buscaino G, Buffa G, Sara G, Bellante A, Tonello AJ Jr, Hardt FAS, Cremer MJ, Bonanno A, Cuttitta A, Mazzola S (2009). Pinger affects fish catch efficiency and damage to bottom gill nets related to bottlenose dolphins. Fish Sci. (Tokyo, Japan). 75(3):537-544.

Choppin GR, Liljenzin JO, Rydberg J (2002). Radiochemistry and Nuclear Chemistry, 3rd Ed., Butterworth-Heinemann (ISBN 978-0-7506-7463-8). 4(13).

Gerhard VDE, Stephen S, Leonel G, Ruben B, Kirsty G (1998). Electric fish measure distance in the dark. Nature 395:890-894.

Hellstrom S, Brune D (1964). Determination of the absolute disintegration rate of 137Cs sources by the tracer method. Nukleonik 6(4):174-178.

Inazu T, Tsunoda A, Ohnishi S, Matsubara Y (2011). Determination of radioactive substances in foods by Ge semiconductor detector. Kenkyu Hokoku - Kagawa-ken Sangyo Gijutsu Senta 12:67-68.

Katsura H (2013a). Accumulation of a specific nuclide by Female Common skete (Feminam Okamejei kenojei spp.). Asian J. Chem. 25(13):7613-7616.

Katsura H (2013b). The Total Quantity of Caesium Radioisotopes in Fish in the Fukushima-Ken Exclusive Economic Zone, Japan, in November 2012. Sci. Res. Essays. 8(26):1252-1257.

Kalmun ADJ (1982). Electric and Magnetic Field Detection in Elasmobranch Fishes. Science 218(26):916-918.

Minatani T, Nagai H, Nakamura M, Otsuka K, Sakai Y (2012). Radioactive cesium analysis in radiation-tainted beef by gamma-ray spectrometry with germanium semiconductor detector. Shokuhin eiseigaku zasshi. J. Food Hyg. Soc. Jpn. 53(4):177-82.

Murray RW (1962). The Response of the Ampullae of Lorenaini of Elasmobranchs to Electrical Stimulation. J. Exp. Biol. 39:119-128.

Thompson SE, Burton CA, Quinn DJ, Ng YC (1972). Concentration factors of chemical elements in edible aquatic organisms. California Univ., Livermore. Lawrence Livermore Lab. UCRL-50564 Rev.1.

Wolfson JL (1956). High-energy forbidden b-ray transitions from cesium-134 cobalt-60, scandium-46, and mercury-203. Can. J. Phys. 34:256-264.

academicJournals

Vol. 11(22), pp. 296-305, 30 November, 2016
DOI: 10.5897/IJPS2016.4546
Article Number: 128344F61633
ISSN 1992 - 1950

http://www.academicjournals.org/IJPS

International Journal of Physical Sciences

Full Length Research Paper

Troubled roads: Application of surface geophysics to highway failures of the sedimentary terrain (Iruekpen-Ifon Road) of Edo State, Nigeria

Ozegin K. O.[1]*, Adetoyinbo A. A.[2], Jegede S. I.[1] and Ogunseye T. T. [2]

[1]Department of Physics, Ambrose Alli University, Ekpoma Edo State, Nigeria.
[2]Department of Physics, University of Ibadan, Ibadan, Nigeria.

Received 2 August, 2016; Accepted 24 October, 2016

As part of effort to examine the factors responsible for highway failure in the sedimentary terrain, geophysical survey involving Very Low Frequency Electromagnetic (VLF-EM), Schlumberger Vertical Electrical Sounding (VES), and dipole-dipole electrical resistivity techniques were carried out along Iruekpen-Ifon highway. This was aimed at using surface geophysics to characterize and identify the factors responsible the for road failures along Iruekpen-Ifon highway. ABEM WADI instrument was used to obtain electromagnetic-Very Low Frequency (VLF) field data, while ABEM resistivity meter was used to obtain electrical resistivity field data. The VLF-EM data were interpreted using the VLF Graphic software, VELFAN 1.0 double plot of filtered real and filtered imaginary against distance. The VES data obtained were interpreted using IP 2 Win software. Geoelectric parameters were used to generate the Dar Zarrouk second order parameters. 2-D inversion modeling of the dipole-dipole data was carried out using ZONDRES window software. VLF-EM result suggested varying degree of conductivity in the area and the wide spread of clay/metallic ore and water in the study area. Results show that the topsoil generally varies in composition from clay to clayey and laterite with resistivity values varying from 89 to 400 Ωm and thickness between 0.2 and 4.0 m. The fractured layers composed of clay and compacted clayey sand which represents the recent alluvial deposits with resistivity values of 2 to 89 Ωm and the thickness between 1.5 and 11 m. The fresh water zone is characterized by low resistivity ranging from 0.5 to 23 Ωm, which is diagnostic of saline water saturated with clay formation, fresh water ingression, and marls. The values of co-efficient of anisotropy (λ) range from 1.03 to 2.19. The relatively higher values of *λ* (1.30 to 2.19) suggest that the subsurface rocks in these areas are likely to be more intensely fractured and more permeable. The saline water saturated with clay formation, fresh water ingression, fracture and marls clearly limit the lithological contacts and enhance high swelling potential which might be responsible for the road pavement failures in the studied area.

Key words: Highway, resistivity, troubled roads, Dar Zarrouk, anisotropy.

INTRODUCTION

A road is a thoroughfare, way, or route on land between two places, which in general has been paved or otherwise, enhanced to allow travel by some transportation. However, the presence of discontinuities such as cracks, surface deformation (rutting, etc.), disintegration (potholes, etc.), surface defects (ravelling, etc.) on a road network is regarded as road failure. Accordingly, roads are constructed with detailed

information obtained from geological, geophysical and geotechnical investigations of the construction site because information obtained play important role in the design, stability, economical construction and maintenance of the roads. Such investigations are capable of delineating structures such as unconsolidated soil formations with varying resistivity and expansiveness, naturally occurring underground water channels which may expedite discontinuities. Degradation of many highway pavements is traceable to the surface water ingress through cracks and joints. These have resulted to frequent motor accidents leading to loss of lives and properties in Nigeria. However, some major Nigerian highways are known to fail shortly after construction and well before their design ages and this unfortunately has become an embarrassing stigma to the road users and nation at large. Furthermore, one of the main consequences of many rackety vehicles on the Nigerian roads is due to its failure. It has been shown that vehicles wear down faster in less developed countries of Africa like Nigeria than is obtainable in civilized economies. This is evident in secondhand vehicles that are shipped from developed economies to Africa which are in most cases here considered as new vehicles.

In particular, three main sections of the Iruekpen-Ifon highway have experienced recurrent failure after rehabilitations. In recognition of the devastating effects of these highway problems in recent years, it has become imperative to use surface geophysics to investigate these failed sections in order to identify the causes of the failures along this highway. Surface geophysics provides economic, non-destructive and rapid tools for the detection of discontinuity in road network resulting in cracks, disintegration, bulges and depressions. There are numerous case studies all over the world showing the effectiveness of geophysical methods in the detection of highway failures (Olorunfemi and Mesida, 1987; Adesida and Omosuyi, 2005; Ozegin et al., 2007; Momoh et al., 2008; Ojo et al., 1990; Soupios et al., 2007; Akintorinwa and Adeusi, 2009; Ofomola et al., 2009); and the methods have been established to play complementary roles in geotechnical studies, besides the fact that they are less expensive and non-invasive.

Road failure is an inevitable consequence of man's activities and a natural phenomenon as well. Road failure can be of these patterns, namely, (i) Alligator cracking, (ii) Rutting, (iii) Chuck holes (Potholes), (iv) Ravelling, and (v) Shear failures (Block cracking).

Alligator cracking

This is described by interconnected cracks forming a series of small polygons resembling an alligator's skin (Figure 1a). This could result from the fatigue effect of repetitive heavy truck loads or ageing in combination with exponential loss of pavement thickness. It can occur with or without surface distortion and pumping.

Rutting

A rut is a longitudinal deformation at wheel tracks mainly associated with shoving along the road (Figure 1b). This is caused by heavy loads and high tyre pressure, subgrade settlement caused by saturation, poor construction methods, or asphalt mixtures of inadequate strength.

Chuck holes (Potholes)

Potholes are irregularly shaped holes of various sizes. These most often result from wear or destruction of the wearing course, sometimes from the presence of foreign bodies in the surfacing (Figure 1c). They can also be caused by water penetrating the surface and causing the base and/or subgrade to become wet and unstable. They are small when they first appear. In the absence of maintenance, they grow and reproduce in rows.

Ravelling

This is progressive loss of pavement material. The possible cause for ravelling could be separation of bituminous film from aggregates through stripping caused by deficiency of bonding or ageing of surface due to variations in climatic and loading conditions (Figure 1d). It can also occur due to the inconsistent deformation of the lower pavement layers.

Shear failures (Block cracking)

This is block cracking leading to chipping of pavement surfacing and/or upheaval outside the tyre cracks with associated cracking. This could result from deficiency in cohesion and internal friction in pavement base structure due to ageing and fatigue (Figure 1e).

MATERIALS AND METHODS

Two geophysical methods were adopted; Very Low Frequency electromagnetic method and electrical resistivity method. ABEM

*Corresponding author. E-mail: ozeginkess@yahoo.com.

Figure 1. (a) Alligator cracking; (b) Rutting at wheel path; (c) Potholes; (d) Ravelling; (e) Block cracking.

WADI instrument was used to obtain electromagnetic-Very Low Frequency (VLF) field data, while ABEM resistivity meter was used to obtain electrical resistivity field data. The use of electromagnetic method was preliminary survey along the three locations with traverses measuring 210, 600 and 140 m, respectively. The EM-VLF data were interpreted using the VLF Graphic software, VELFAN 1.0 double plot of filtered real and filtered imaginary against distance. For the electrical resistivity method, two techniques were used, namely, the Vertical Electrical Sounding (VES) using Schlumberger configuration with AB/2 (AB/2 = Current electrode spacing) varying from 1 to 100 m. A total of 42 VES stations were occupied, which include 10, 25 and 7 VES stations at the three studied locations, respectively. 2-D Electrical Resistivity Tomography (ERT) using dipole-dipole configuration with inter station separation (a) of 10 m, an expansion factor (n) that varied from 1 to 5 was also carried out. The VES data obtained were interpreted using IP 2 Win Software and layer parameters such as true resistivity and thickness were determined. The geoelectric parameters were used to generate the concept of Dar Zarrouk second order (Maillet, 1974) parameters (transverse unit resistance, longitudinal conductance and resistivity ρ (Ω-m) for the co-efficient of anisotropy (λ) in porous media). 2-D inversion modeling of the dipole-dipole data was carried out using ZONDRES window software. It should be emphasized that 2 D Electrical Resistivity Tomography (ERT) is a method by which 2 Dimensional images of subsurface resistivity distribution are generated. Using this method, features with electrical properties differing from those of the surrounding material may be located and characterized in terms of electrical resistivity, geometry and depth of burial.

Location and geological setting of the study area

The study area is bounded by Longitudes 5°50' and 6°39'E and Latitudes 6°55' and 7°37'N (as shown in Figure 2). The study area is underlain by the Imo Eusterine and Marine Shale which comprise grey-black shale at the basal region of the section of about 100 m, graded upward into alternation of thin beds of fissile dirty-light shale and gypsum of about 2 to 5 cm. The section passes on into light yellow-brown sandy mudstone with lateral variation in faces from

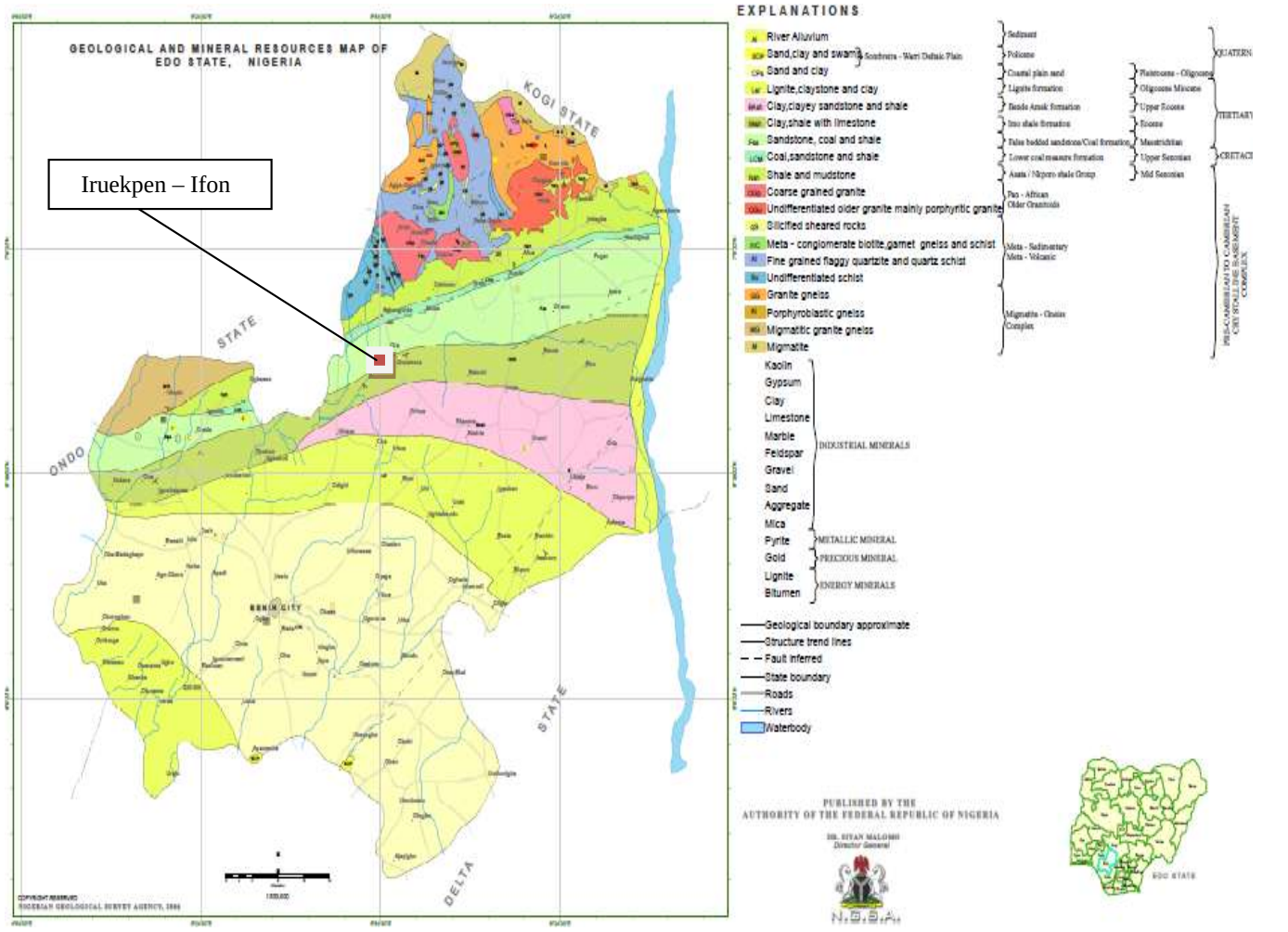

Figure 2. Geological and mineral resources map of Edo State, NGSA 2006.

sandy mudstone to clay. The shale is generally hard at Uhonmora and the section is more of shale and intercalation of gypsum and shale towards the top of the section. However, the Ozalla section of the Imo Shale does not have intercalation of gypsum bed with shale rather it comprises mudstone, clay and shale (Plate 1). The two sections of Imo Shale in the study area exhibit similar unique characteristic of ferruginous nature within the sandy mudstone unit. This unique characteristic in the study area strengthening the load carrying capacity of the lithology except for the area with faces variation from ferruginous sandy mudstone to clay. The mudstone is well laminated with imbedded clay clast (Obaje, 2009).

Sedimentation in the Lower Benue Trough commenced with the marine Albian Asu River Group, although some pyroclastics of Aptian-Early Albian ages have been sparingly reported (Ojoh, 1992). The Asu River Group in the Lower Benue Trough comprises the shales, limestones and sandstone lenses of the Abakaliki Formation in the Abakaliki area and the Mfamosing Limestone in the Calabar Flank (Petters, 1982). The marine Cenomanian–Turonian Nkalagu Formation (black shales, limestones and siltsones) and the interfingering regressive sandstones of the Agala and Agbani Formations rest on the Asu River Group. Mid-Santonian deformation in the Benue Trough displaced the major depositional axis westward which led to the formation of the Anambra Basin. Post-deformational sedimentation in the Lower Benue Trough, constitutes the Anambra Basin. Sedimentation in the Anambra Basin, thus commenced with the Campanian-Maastrichtian marine and paralic shales of the Enugu and Nkporo Formations, overlain by the coal measures of the Mamu Formation (Reijers and Nwajide, 1998). The fluviodeltaic sandstones of the Ajali and Owelli Formations lie on the Mamu Formation and constitute its lateral equivalents in most places. In the Paleocene, the marine shales of the Imo and Nsukka Formations were deposited, overlain by the tidal Nanka Sandstone of Eocene age. Down dip, towards the Niger Delta, the Akata Shale and the Agbada Formation constitute the Paleogene equivalents of the Anambra Basin.

RESULTS AND DISCUSSION

The approaches adopted for data interpretation are of two types, namely qualitative approach which involves visual inspection of Electromagnetic curves and quantitative approach which involves depth calculation of VES, dar Zarrouk parameters etc. The localities studied are variously shown in (Plate 2a to c).

The purpose of Very Low Frequency – Electromagnetic

Plate 1. Geological setting showing beddings and faults of the rock exposures.

Method (VLF – EM) is to qualitatively delineate the conductive zones and non-conductive zones in the study area. Graphic software, VELFAN 1.0 developed by Alberg Services Nigeria Limited (Geophysical Consulting Services), in MATLAB graphical user interface was used to plot the filtered imaginary and real Very Low Frequency- Electromagnetic curves. High positive values indicate presence of conductive subsurface structures while low or negative values are indicative of resistive formations, (Sharma and Baranwal, 2005).

The positive peak anomalies P1, P2, P3 and P4 on the filtered real curve, revealed vertical and/ or near vertical conductors (Figure 3a).

In Figure 3b, the filtered real curve indicates conductors with positive peaks. P1, P2, P3, P4, P5, P6, F1, F2 and F. These conductors are 80, 175, 212, 245, 380, 420, 500, 522 and 550 m from the starting station (zero mark) of the survey profile.

In Figure 3c, the positive peaks anomalies P1, P2, P3 , P4 and P5 indicated on filtered real curve, show locations of vertical and/or near vertical conductors. These anomalies are 42, 102, 143, 169 and 200 m from the starting station (zero mark) of the survey profile.

Estimating Dar Zarrouk (D-Z) parameters from (VES) results

The analysis of the D-Z parameters longitudinal unit conductance (S), transverse unit resistance (T), also, longitudinal resistivity (ρ_t) provides a very convenient and easily applicable solution to understand the geophysical behavior of saline and fresh water aquifers. (Maillet, 1947) termed the Dar Zarrouk (D-Z) parameters. The secondary parameters (longitudinal conductance (S_i), transverse resistance (T_i), longitudinal resistivity (ρ_L), transverse resistivity (ρ_t) and coefficient of anisotropy (λ)) were determined from the layers' resistivities and thicknesses using the mathematical relations (Zohdy et al., 1974):

$$S_i = \sum_{i=1}^{n} \frac{h_i}{\rho_i} \quad (1)$$

$$T_i = \sum_{i=1}^{n} h_i \rho_i \ (\text{Ohm.m}^2) \quad (2)$$

$$\rho_L = \sum_{i=1}^{n} \frac{h_i}{s_i} \quad (\rho_l = H/S) \quad (3)$$

$$\rho_t = \sum_{i=1}^{n} \frac{T_i}{h_i} \quad (\rho_t = T/H) \quad (4)$$

$$\lambda = \sqrt{\frac{\rho_t}{\rho_L}} \quad (5)$$

The concept of Dar Zarrouk parameters were first introduced by Maillet (1974) to explain the problem of non-uniqueness in the interpretation of resistivity depth sounding curves. As resistivities of clay with sand and saline water interfere with each other, the data

Plate 2. (a) Failed Section at Locality 1; (b) Failed Section at Locality 2; (c) Failed Section at Locality 3.

interpretation becomes a difficult task. Such situation requires the formulation of better analysis technique of interpretation for the existing data to yield useful and easily understandable solution to differentiate among fresh and saline aquifers.

The geoelectric parameters were used to generate the concept of Dar Zarrouk second order parameters. The coefficient of anisotropy *(λ)* has been shown to have

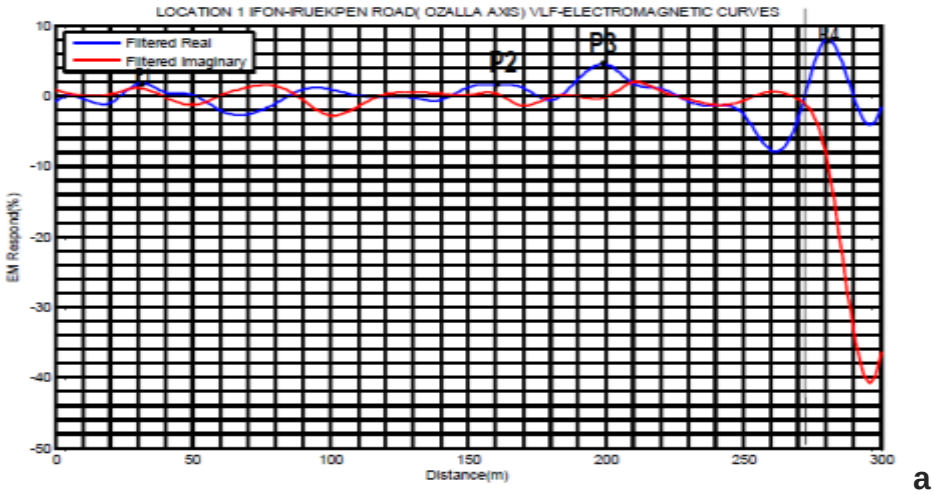

a

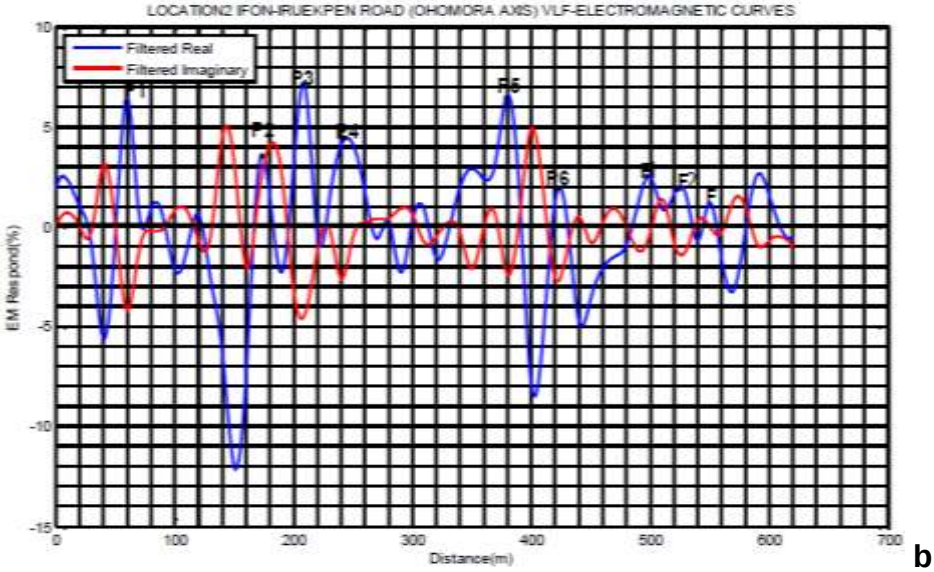

b

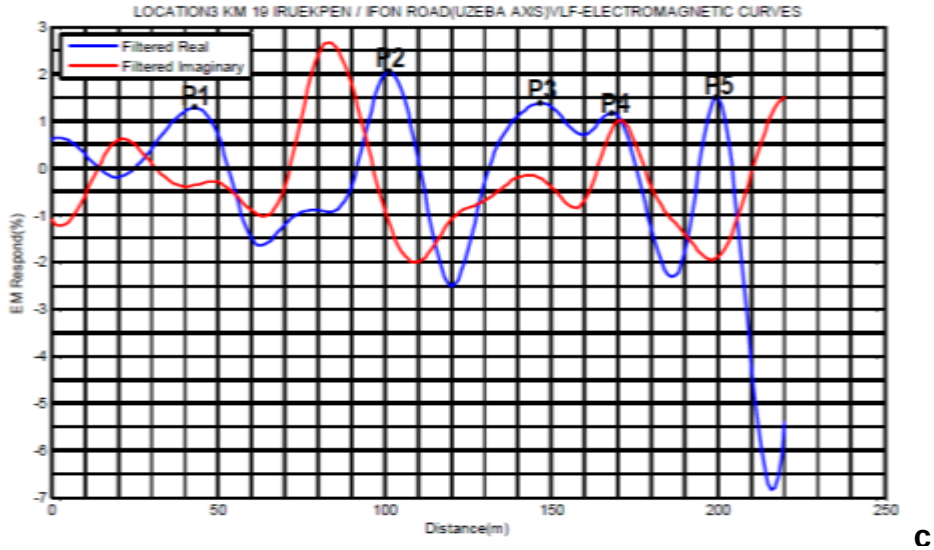

c

Figure 3. (a) VLF-EM Curves in locality 1; (b) VLF-EM Curves in locality 2; (c) VLF-EM Curves in locality 3.

Table 1. Dar Zarrouk parameters results.

VES No.	Total resistance (T)	Total conductance (S)	Co-efficient of anisotropy (λ)
1	115.40	0.017	1.03
2	274.73	0.063	1.20
3	87.31	0.027	1.07
4	654.08	0.144	1.05
5	114.21	0.015	1.24
6	226.13	0.068	1.13
7	102.79	0.128	1.51
8	153.28	0.019	1.38
9	376.84	0.013	1.15
10	851.87	0.007	1.29
11	284.50	0.057	1.16
12	548.80	0.019	1.36
13	583.52	0.024	1.31
14	380.82	0.036	1.31
15	289.81	0.067	1.22
16	279.80	0.070	1.21
17	190.99	0.037	1.12
18	564.75	0.013	1.61
19	181.87	0.081	1.24
20	223.41	0.061	1.14
21	191.51	0.033	1.42
22	175.93	0.033	1.42
23	158.91	0.050	1.33
24	193.62	0.022	1.22
25	230.88	0.030	1.17
26	235.05	0.066	1.28
27	200.85	0.028	1.22
28	414.04	0.023	1.28
29	380.38	0.026	1.29
30	425.75	0.022	1.16
31	245.12	0.026	1.11
32	225.23	0.118	1.12
33	454.77	0.121	1.50
34	353.53	0.047	1.37
35	273.82	0.020	1.06
36	2212.63	0.008	1.53
37	1313.04	0.015	1.43
38	533.34	0.035	1.84
39	163.94	0.070	1.24
40	196.27	0.083	1.33
41	330.10	0.022	2.19
42	150.45	0.019	1.09

the same functional form as permeability anisotropy. Thus, a higher coefficient of anisotropy *(λ)* implies higher - permeability anisotropy. The values of co-efficient of anisotropy (λ) ranges from of 1.03 to 2.19 (Table 1). The relatively higher values of *λ* (1.30 to 2.19) suggest that the subsurface rocks in these areas are likely to be more intensely fractured and more permeable. These clearly limit the lithological contacts and enhance high swelling potential.

The dipole-dipole profiling involving the combination of horizontal profiling and vertical electrical sounding was adopted as a means of mapping vertical discontinuities

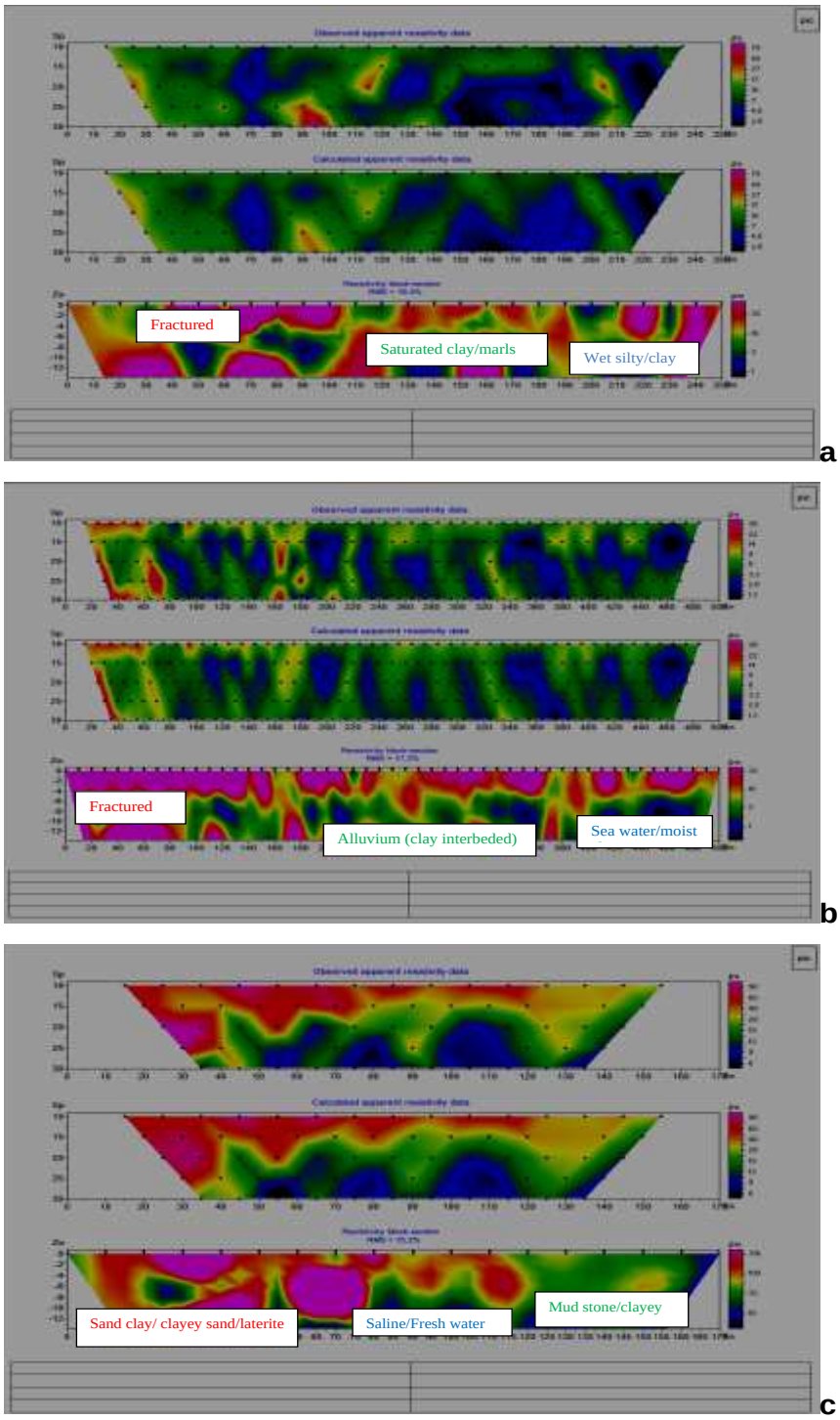

Figure 4. (a) 2-D Modelling of Dipole-Dipole Data at Locality 1; (b) 2-D Modelling of Dipole-Dipole Data at Locality 2; (c) 2-D Modelling of Dipole-Dipole Data at Locality 3.

typical of jointed, fractured and faulted zones. The dipole-dipole field data were inverted to 2-D resistivity structure using 'ZONDRES for Window' software. The dipole-dipole pseudo-sections and the 2-D resistivity structures are variously shown in Figure 4a, b and c.

The dipole-dipole pseudo-sections and the 2-D resistivity structure at locality 1 are as shown in Figure 4a. The 2-D resistivity structure shows a subsurface

sequence with very thin topsoil which is virtually unrepresented on the 2-D resistivity structure, a nearly uniform weathered layer and nearly filled entire structure with wet silty/clay and saturated clay/marls. The dipole-dipole pseudo-sections (field and theoretical) and 2-D resistivity structure at locality 2 (as shown in Figure 4b), shows a fracture/weathered basement, moist clay and alluvium that are predominately observe with depth varying from 1 to 12 m. Figure 4c shows the dipole-dipole pseudo-sections and 2-D resistivity structure profile at locality 3. The 2-D resistivity structure shows a subsurface sequence that is composed of thin topsoil (unrepresented), a variably thick clayey sand/laterite layer, soils and waters (containing fresh water, clayey sand, saline and mud stone).

Conclusion

From the engineering geophysical site investigation undertaken at the study areas (locations 1, 2 and 3), it can be inferred that the possible causes of highway pavement failure in the studied highway are near-surface linear (geological) features such as lithological contact beneath the highway pavements. This feature act as zone weakness that enhances the ingression (accumulation) of water and hence leading to pavement failure portions at all the locations, which is secondary salinity. Marls and clay topsoils/sub-grade soils (with characteristic low layer resistivity less than 100 Ωm) which are encased in alluvium have the tendency of absorbing water as a result of intense fracture hence exhibit high swelling potential and collapse under imposed traffic load stress which subsequently lead to translational failure. This fracture could also be said to be non-systematic and first order. This was majorly observed in failed portion 2. Excessive cut into the conductive water absorbing clayey substratum (weathered layer) that is montmorillonite (clay that undergoes expansion and contraction by virtue of change in moisture contents) as observed at locations 1 and 3. Potential to degrade the pavement material is the presence of water (permanent or seasonal) in the road environment, may have a far more deleterious impact on the road formation than salts present in the water. This was visibly seen in location 2.

Conflict of Interests

The authors have not declared any conflict of interests.

REFERENCES

Adesida A, Omosuyi GO (2005). Geoelectric investigation of Bedrock Structures in the Mini-Campus of The Federal University of Technology, Akure, Southwestern Nigeria and the Geotechnical Significance. Nig. J. Pure Appl. Phys. 4:32-40.

Akintorinwa OJ, Adeusi FA (2009). Integration of geophysical and geotechnical investigation for a proposed lecture room complex at the Federal University of Technology, Akure, SW, Nigeria. J. Appl. Sci. 2(3):241-251.

Maillet R (1974). The fundamental equations of electrical prospecting. Geophysics 12(4):529-556.

Momoh LO, Akintorinwa OJ, Olorunfemi MO (2008). Geophysical Investigation of Highway Failure – A case Study from the Basement Complex Terrain of Southwestern Nigeria. J. Appl. Sci. 4(6):637-648.

Obaje NG (2009). Geology and Mineral Resources of Nigeria (Lecture Notes in Earth Sciences Series, Volume 120).

Ofomola MO, Adiat KAN, Olayanju GM, Ako BD (2009). Integrated geophysical methods for post foundation studies, Obanla Staff Quarters of the Federal University of Technology, Akure Nigeria. Pac. J. Sci. Technol. 10(2):93-110.

Ojo JS, Ayangbesan TA, Olorunfemi MO (1990). Geophysical survey of a dam-site: A case study. J. Mining Geol. 26(2):201-206.

Ojoh KA (1992). The Southern part of the Benue Trough (Nigeria) Cretaceous stratigraphy, basin analysis, paleo-oceanography and geodynamic evolution in the equatorial domain of the South Atlantic. NAPE Bull. 7:131-152.

Olorunfemi MO, Mesida EA (1987). Engineering Geophysics and its application in Engineering Site Investigation-(case study from Ile-Ife area). Nig. Eng. 22(2):57-66.

Ozegin KO, Azi SO, Isiwele DO (2007). Geophysical Investigation of Oke-Agbe-Oyin Road Failure Using VLF and Double Dipole. J. Nig. Assoc. Math. Phys. 11:411-414.

Petters SW (1982). Central West African Cretaceous-Tertiary benthic foraminifera and stratigraphy. Palaeontographica Abt. A 179:1–104.

Reijers TJA, Nwajide CS (1998). Geology of the Southern Anambra Basin. Unpublished Report for Chevron Nigeria Limited. Field Course Note.

Soupios PM, Georgakopoulos P, Papadopoulos N, Saltas V, Andreadakis A, Vallianatos F, Sarris A, Makris JP (2007). Use of engineering geophysics to investigate a site for a building foundation. J. Geophys. Eng. 4:94-103.

Sharma SP, Baranwal VC (2005). Delineation of groundwater-bearing fracture zones in hard rock area integrating VLF-EM and resistivity data. J. Appl. Geophys. 57:155-166.

Zohdy AAR, Eaton GP, Mabey DR (1974). Application of surface geophysics to groundwater investigations: Techniques of water resources investigations of the United Geophysical Survey Book. United States Government Printing Office, Washington DI, P 116.

academicJournals

Vol. 11(22), pp. 306-320, 30 November, 2016
DOI: 10.5897/IJPS2016.4565
Article Number: 18FBFB161635
ISSN 1992 - 1950

http://www.academicjournals.org/IJPS

International Journal of Physical Sciences

Full Length Research Paper

Thermo-economic study of hybrid cooling tower systems

Sonia Parsa[1], Hossein Shokouhmand[2]*, Amirmohammad Sattari[2], Mohammad Nikian[1] and Fatemeh Entezari Heravi[2]

[1]Islamic Azad University of Takestan, Iran.
[2]School of Mechanical Engineering, College of Engineering, University of Tehran, Tehran, Iran.

Received 19 September, 2016; Accepted 13 October, 2016

In this paper, the effects of ambient temperature and relative humidity on performance of wet, dry, and two combined cooling systems are studied for a typical 250 MW power plant in Hamedan, Iran. Although there have been many works in background of effects of different parameters on performance of cooling towers, there is no detail analysis about different alternatives of hybrid cooling systems due to the water consumption. In this study, four alternatives were considered for the cooling system: wet, dry, and two combined wet and dry cooling systems. One of the hybrid systems demanding only half of the cells of the existing wet cooling system so has a limitation for water consumption. Another one has no limitation for utilizing all of the cells of the existing wet cooling towers and as a result does not have any limitation for water consumption. Investigating mentioned cases are significant due to the lack of water in middle-east countries. Also, by means of monthly profiles of ambient temperature, the amount of annual power loss is computed for each case. The water consumption for each case, is computed as well. Finally, the best alternative was determined by computing both the capital and annual costs, and annual water consumption.

Key words: Wet cooling tower, dry cooling tower, hybrid cooling tower, power plant, economic evaluation.

INTRODUCTION

Cooling towers are among the most important components of power plants. They are utilized to reduce the augmented temperature of water in power plants and return the cold water into the main plant cycle. Cooling agent in these towers can be either air or water that, with either direct or indirect contact, reduces the temperature of hot water coming from the condenser. Cooling towers are classified into three different types based on their heat transfer approach, wet, dry, and combined cooling towers. Wet cooling towers operate upon evaporative cooling. The working fluid and the evaporated fluid are the same in these towers. Dry cooling towers operate with a surface that intercepts the working fluid from the ambient air, which is used for convective heat transfer. The dry cooling towers do not use evaporation as a means for cooling; therefore, they consume much less

*Corresponding author. E-mail: hshokoh@ut.ac.ir.

water. According to the water shortage problem in Iran, replacement of wet cooling towers with dry ones seems an attractive approach. So, the influence of different parameters on the performance of cooling towers is a major issue for designers.

Among different parameters which affect the performance of cooling towers, ambient temperature and relative humidity are the most influential. So, there are many works done in this background. In 1946, one of the first investigation of performance of cooling towers has been conducted by Simpson and Sherwood (1946). They found constants for evaluating coefficient of mass transfer. Berman was the first one who described how the Log-Mean Enthalpy Method (LMED) may be applied to cooling tower design (Berman, 1961). Besides, Moffat (1966), for the first time derived the ε-NTU equation for a counter-flow cooling tower. Furthermore, Jaber and Webb (1989) developed the ε-NTU design method for cooling towers. They presented sample calculations for counter and cross-flow cooling towers. Also, the authors summarized the LMED method introduced by Berman, and show that this is totally consistent with the ε -NTU method. Bernier (1995) reviewed the heat and mass transfer processes in cooling towers. He also presented a practical correlation for evaluating water evaporation rate affiliated with mass transfer at the water-air interface. In other research Söylemez (2004), for the first time optimized the water to air mass ratio for counter flow cooling towers that included the ambient pressure and average of tower and basin temperature of cooling towers in detail. Muangnoi et al. (2008) investigated the influence of temperature and humidity on performance of counter-flow wet cooling towers by using exergy analysis and finally by utilizing optimization methods, best temperature and humidity for achieving the highest efficiency were computed. Also, Lucasa et al. (2010) due to disadvantages of the moisture that goes out from cooling towers, worked on the effect of psychometric environmental conditions on the amount of the afore-mentioned moisture. They concluded that by increasing dry-bulb temperature, the amount of the moisture escaping from the tower declines. In another research, Papaefthimiou et al. (2012) studied thermodynamic effect of ambient temperature on specifications of the cooling towers. They resulted that by decreasing inlet wet-bulb temperature, the temperature will be more reduced in the tower; as well as the amount of waste of water. In other work He et al. (2014) investigated the influence of environmental conditions and water flow on performance of cooling towers with pre-cooled air. They found that influence of water flow on performance of cooling towers is negligible. Also, it was concluded that employing this type of cooling towers, under the conditions of high ambient temperature and low humidity is very helpful. And finally the evaporation rate of water in this type of towers is lower than wet cooling towers. Thereafter Ma et al. (2015) surveyed the effect of both the ambient temperature and cross wind on efficiency of cooling towers. They concluded that effect of outlet water temperature has non-linear and linear relationship with the wind velocity and the ambient temperature respectively. Finally, He et al. (2015) performed experimental study on application of two trickle media for inlet air pre-cooling of natural draft cooling towers. They optimized size of trickles which has the less pressure drop and the highest performance. Another major parameter that affect performance of cooling towers, especially natural-draft cooling towers, is wind that widely considered in many works (Harnach and Niemann, 1980; Dachun and Chenxin, 1987; du Preez and Kröger, 1995; Su et al., 1999; Al-Waked and Behnia, 2004; Ke and Ge, 2014). Since the mean wind speed of the target site of the current research is low, and dry cooling system is one of the alternatives of this research, effect of wind speed is not considered.

Another topic that attracted many attentions is to utilizing saline water in cooling tower systems. For instance, Kinnon et al. (2010) showed that NaCl is the main salt in the saline water from coal-bed methane production. Sadafi et al. (2015a) monitored the saline water droplet size at different ambient conditions using microscope digital camera. They showed that for 500 µm radius droplets with 3 and 5% initial NaCl mass concentrations the net energy required to evaporate the droplet falls by 7.3 and 12.2%, respectively (compared to a pure water droplet). Also, in a subsequent study, Sadafi (2015b) investigates the performance of saline water, compared to pure water in spray cooling and demonstrates the existence of several advantages.

In the current research, four cases are considered for the cooling system of a typical power plant, with a nominal capacity of 250 MW placed in Hamedan city in Iran. These cases are utilizing wet cooling towers, dry cooling towers and two combined wet and dry systems (hybrid systems), which in one case there is a limitation of using wet cooling towers due to lack of water sources in the region, while there is no limitation in another case. Utilizing dry and combined cooling systems are important issues due to lack of water in the world, especially in Iran. Hence, in the present work, at first, thermodynamics of wet and dry cooling towers are studied. Then, the effects of ambient temperature and relative humidity on the performance of wet and dry cooling towers are investigated. Using profiles of ambient temperature and relative humidity of Hamedan power plant, diagrams relevant to the performance of wet, dry and combined cooling towers are extracted. Finally, four mentioned cases are compared by the economical aspect and the best one is determined.

PRESENT MODEL

In this paper, four alternatives are considered for cooling

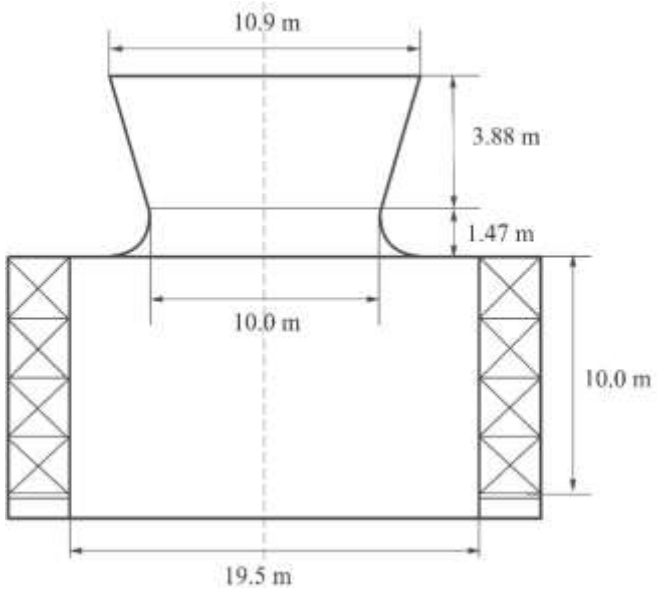

Figure 1. Scheme of the present wet cooling tower.

Table 1. General specifications in the design of the wet cooling tower.

Parameter	Value
Number of cells	12
Water inlet temperature	38.2°C
Water outlet temperature	27.8°C
Wet bulb temperature	14.5°C
Maximum air flow rate	889150 (cfm/cell)
Quantity of make-up water (at 35% RH)	675.6 (m^3/h)

system of a typical power plant with 250 MW nominal capacity. These alternatives are

A) Wet cooling towers
B) Dry cooling towers
C) Wet/dry system with 50% capacity of wet cooling towers
D) Wet/dry system which in any conditions power plant work with full load capacity.

Case A

This case contains a series of wet cooling systems including twelve wet cooling towers. Dimensions of present wet cooling towers and specifications are presented in Figure 1 and Table 1 respectively.

Case B

In this case, cooling system contains a dry cooling tower. Geometry and general specifications of dry cooling tower of the current work are illustrated in Figure 2 and Table 2 respectively. It should be noted that there is no auxiliary system (such as peak coolers) in studied dry cooling towers.

Case C

In this case, as shown in Figure 3, cooling water, first, enters a dry cooling tower, and, next, enters a shell and tube heat exchanger. Half of the present wet cooling towers (6 cells) supply the cooling water of the heat exchanger. So, in this case, limitation of water consumption, due to presence of wet cooling towers, confines the accessibility to the full capacity of wet cooling system (12 cells). So it is expected that, in this particular case, power losses occur at high ambient temperatures. It should be noted that the specifications of wet and dry cooling towers in this case are similar to those of cases A and B.

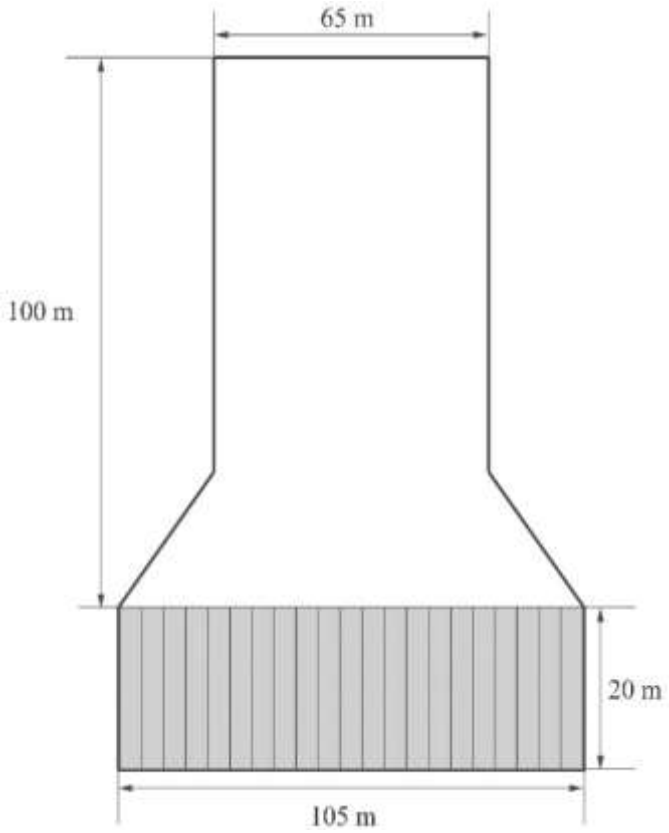

Figure 2. Geometry model of the dry cooling tower of the work.

Table 2. General specifications of the dry cooling tower.

Parameter	Value
Number of deltas	120
Height of deltas	20 m
Tower height (from base)	120 m
Base diameter of tower	105 m
Upper diameter of tower	65 m
Cooler surface	8,000 m^2
Cooling capacity	28,000 m^3/h

Case D

Difference of this case with case C is that the limitation of make-up water is not considered. So, in case D, at high ambient temperature conditions, more wet cooling towers come into the cooling system and compensate amount of power losses which happens in case C. It should be noted since the dry cooling tower is present in this case, all of the wet cooling towers will not be utilized even at the high temperatures. So, the amount of water usage in this case is lower than case A. The number of cells utilized in any ambient temperature is dependent on the requisite cooling capacity to achieve to the full load capacity of the power plant (250 MW). It means that in higher ambient temperature more cells will be utilized in order to achieve to the desired cooling capacity.

MATHEMATICAL MODELS

Dry cooling tower modeling

Governing equations that are utilized in this work for thermodynamic analysis of dry cooling tower are heat transfer in heat exchangers and energy conservation. A brief description of mentioned governing equations is presented in the following.

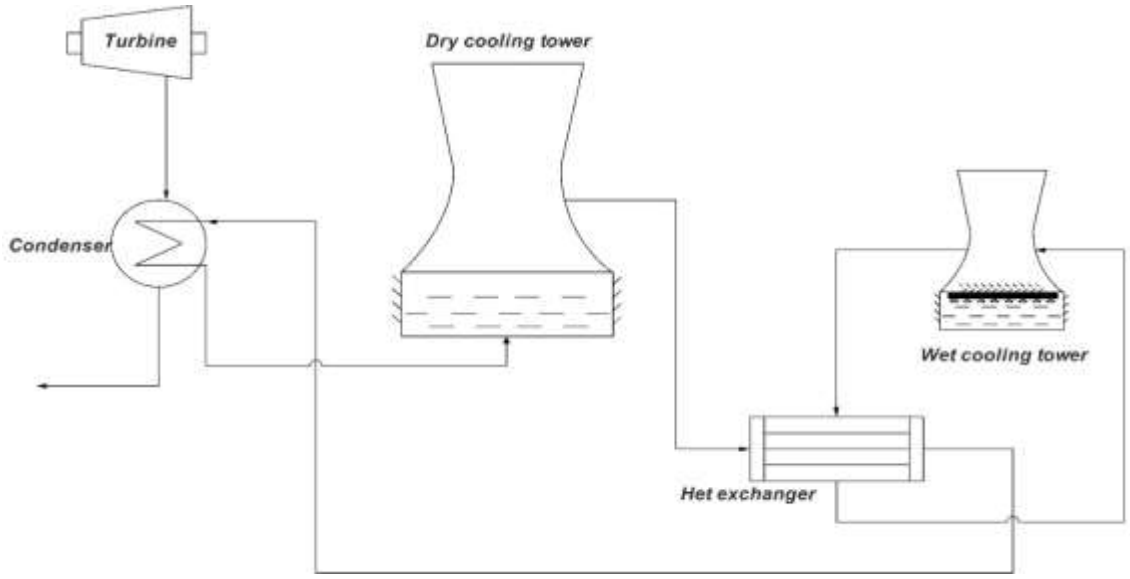

Figure 3. Schematic of the current combined system.

Heat transfer equations

It is common to use Forgo T60 type heat exchangers in dry cooling towers. Total heat transfer coefficient includes three different heat transfer coefficients including convection of internal water flow, conduction from tubes, and convection between air and tubes. So, Equation (1) can be considered for determining the total heat transfer coefficient.

$$\frac{1}{U} = \frac{1}{h_{w,i}A_i} + \frac{1}{\eta h_{a,f}A_f} + \frac{\delta}{KA_t} \quad (1)$$

Calculating heat transfer of dry cooling towers based on front surface is a common approach. So, Equation (1) can be rewritten as Equation (2).

$$\frac{1}{U_C(A_f/A_{fr})} = \frac{1}{h_{w,i}(A_i/A_{fr})} + \frac{1}{\eta h_{a,f}(A_f/A_{fr})} + \frac{\delta}{K(A_t/A_{fr})} \quad (2)$$

Considering that dimensions of Forgo T60 heat exchangers are specified, in order to simplify equations, Equations (3) to (5) are assumed,

$$h_w = h_{w,i}\left(\frac{A_i}{A_{fr}}\right) \quad (3)$$

$$h_a = \frac{1}{\left[\frac{1}{\eta h_{a,f}\left(A_f/A_{fr}\right)} + \frac{\delta}{K\left(A_t/A_{fr}\right)}\right]} \quad (4)$$

$$U = U_C\left(\frac{A_f}{A_{fr}}\right) \quad (5)$$

So:

$$\frac{1}{U} = \frac{1}{h_w} + \frac{1}{h_a} \Rightarrow U = \frac{h_w h_a}{h_w + h_a} \quad (6)$$

In above equations, total heat transfer was considered for clean tubes, and effect of fouling has not been not included. For considering fouling, total heat transfer can be modified as Equation (7).

$$\frac{1}{U_{dirty}} = \frac{1}{U_{clean}} + R_f \quad (7)$$

As a result,

$$U_{dirty} = \frac{U_{clean}}{U_{clean}\,R_f + 1} \quad (8)$$

R_f is sediment coefficient. For Forgo heat exchangers in dry cooling systems R_f is considered to be $0.00009\ \frac{m^2C}{W}$ (Know HowDocuments, 1984).

Combining Equations 6 and 8, total heat transfer can be calculated through Equation 9.

$$U = \frac{h_w.h_a}{h_w + h_a + R_f.h_w.h_a} \quad (9)$$

In order to calculate water and air side heat transfer coefficients (h_w, h_a), Equation (10) has been presented by the manufacturer of Forgo T60 heat exchangers (Know HowDocuments, 1984)

$$h_w = [317.3 + 2.82(T_{wi} + T_{wo})]Q_{ow}^{0.8}$$
$$h_a = 1180\left[\frac{\dot{m}_a}{A_f}\left(\frac{\rho_{oa}}{\rho_{am}}\right)^{0.64}\right]^{0.515} \quad (10)$$

ρ_{ma} is average air specific mass through a heat exchanger that is equal to:

$$\rho_m = \frac{\rho_{a,i} + \rho_{a,o}}{2} \quad (11)$$

Energy conservation

Forgoing heat losses in plumbing and water transfer route from the condenser to the tower, heat released from vapor to the cooling liquid in condenser is equal to the heat released from cooling tower water. The released heat from cooling water is equal to the absorbed heat by the passing air from tower. So,

$$\dot{Q}_c = \dot{m}_{w,t} C_{p_w} \Delta T_w = \dot{m}_{a,t} C_{p_a} \Delta T_a \quad (12)$$

$\dot{Q}_C$ is released heat from condenser which based on number of deltas and pass flow rate from a column can be written as follows:

$$\dot{Q}_c = 2N_d \dot{m}_w C_{p_w} \Delta T_w = 2N_d \dot{m}_a C_{p_a} \Delta T_a \quad (13)$$

Wet cooling tower modeling

The control volume of a counter flow cooling tower is illustrated in Figure 4. The most important assumptions are summarized as follows:

1) Heat and mass transfer occur only in the perpendicular direction of the flows.
2) Losses of heat and mass transfer through tower walls are neglected.
3) Mass transfer coefficient is constant all over the tower.
4) The water temperature distribution is uniform in each cross section.
5) The tower cross section is constant in every height.
6) The Louis factor is considered as a variable in the modeling.

The conservation of mass equation for the entering water into the air in the steady state is indicated by Equation (14).

$$\dot{m}_a W + h_D A_V dV \left(W_{s,w} - W\right) = \dot{m}_a \left[W + \left(\frac{\partial W}{\partial V}\right) dV\right] \quad (14)$$

In which *dV* is the control volume element which can be seen in Figure 4.

Equation (14) is simplified as,

$$\dot{m}_a dW = h_D A_V dV \left(W_{s,w} - W\right) \quad (15)$$

The general energy balance equation of the moist air could be expressed as Equation (16).

$$\dot{m}_a h + h_c A_V dV (T_w - T) + h_D A_V h_{fg,w} dV \left(W_{s,w} - W\right) = \dot{m}_a \left[h + \left(\frac{\partial h}{\partial V}\right) dV\right] \quad (16)$$

After simplification, Equation (16) would be rewritten as

$$\dot{m}_a dh = h_c A_V dV (T_w - T) + h_D A_V h_{fg,w} dV \left(W_{s,w} - W\right) \quad (17)$$

The energy balance for water could be expressed as a function of heat (h_C) and mass (h_D) transfer coefficients,

$$\left[\dot{m}_w + \left(\frac{\partial \dot{m}_w}{\partial V}\right) dV\right] \left[h_{f,w} + \left(\frac{\partial h_{f,w}}{\partial V}\right) dV\right] = \dot{m}_w h_{f,w} + h_c A_V dV (T_w - T) + h_D A_V h_{fg,w} dV \left(W_{s,w} - W\right) \quad (18)$$

The simplified equation would be,

$$\dot{m}_w . dh_{f,w} + \dot{m}_a dW . h_{f,w} = h_c A_V dV (T_w - T) + h_D A_V h_{fg,w} dV \left(W_{s,w} - W\right) \quad (19)$$

By inserting the Louis factor, $Le_f = {h_c}/{h_D c_{p,a}}$ in Equation 19, and a little bit simplification, the Equation (20) is obtained.

$$\dot{m}_w . dh_{f,w} + \dot{m}_a dW . h_{f,w} = h_D . A_V . dV . \left[Le_f . C_{p,a} . (T_w - T) + h_{fg,w} . \left(W_{s,w} - W\right)\right] \quad (20)$$

Combining the aforementioned equations, Equation (21) is derived.

$$\frac{dh}{dW} = \frac{\left(Le_f . c_{p,a} . (T_w - T) + h_{fg,w} . \left(W_{s,w} - W\right)\right)}{W_{s,w} - W} \quad (21)$$

Again, a simplification would result in derivation of Equation (22).

$$h_{s,w} - h = c_{p,a}(T_w - T) + h_g^0 (W_{s,w} - W) \quad (22)$$

By assuming constant specific heat capacity for air in the preceding equations, the Equation (23) is obtained.

$$h_{s,w} - h = c_{p,a}(T_w - T) + h_g^0 (W_{s,w} - W) \quad (23)$$

Ultimately, inserting Equation 23 in Equation 22 and succeeding simplifications will result in the Equation 24.

$$\frac{dh}{dW} = Le_f \frac{\left(h_{s,w} - h\right)}{\left(W_{s,w} - W\right)} + \left(h_{fg,w} - h_g^0 . Le_f\right) \quad (24)$$

Equation 25 indicates the steady state energy balance between the water and air.

$$\dot{m}_a dh = \dot{m}_w dh_{f,w} + \dot{m}_a dW h_{f,w} \quad (25)$$

Be careful that the last term in Equation 25 indicates the impact of water evaporation on the energy equation and $\dot{m}_w$ represents the mass flow rate of water in any altitude of the tower. Commonly, because of the low percentage of water vapor in the air, the diminution in water flow rate is neglected in the modeling (ASHRAE, 1975) and $\dot{m}_w = \dot{m}_{w,in} = \dot{m}_{w,out}$; However, in the present work, in order to increase the accuracy of evaluating losses, these changes have been considered.

$$\dot{m}_a dh = \left(\dot{m}_{w,in} - \dot{m}_a (W_{out} - W)\right) dh_{f,w} + \dot{m}_a dW h_{f,w} \quad (26)$$

It is clear that $dh_{f,w}=C_{p,w}dT_w$. By substituting this in Equation (26) and then in Equation 24, Equation 27 is achieved.

$$\left(\dot{m}_{w,in} - \dot{m}_a (W_{out} - W)\right) \frac{dh_{f,w}}{dW} = \frac{dh}{dW} - h_{f,w} \Rightarrow \frac{dh_{f,w}}{dW} = \frac{1}{\left(\dot{m}_{w,in} - \dot{m}_a (W_{out} - W)\right)} \left[Le_f \frac{\left(h_{s,w} - h\right)}{\left(W_{s,w} - W\right)} + \left(h_{fg,w} - h_g^0 . Le_f\right) - h_{f,w}\right] \quad (27)$$

Finally, Equations 28 to 30 will be used for the simulation of the cooling tower core:

$$\dot{m}_a dW = h_D A_V dV (W_{s,w} - W) \quad (28)$$

$$\frac{dh}{dW} = Le_f \frac{\left(h_{s,w} - h\right)}{\left(W_{s,w} - W\right)} + \left(h_{fg,w} - h_g^0 . Le_f\right) \quad (29)$$

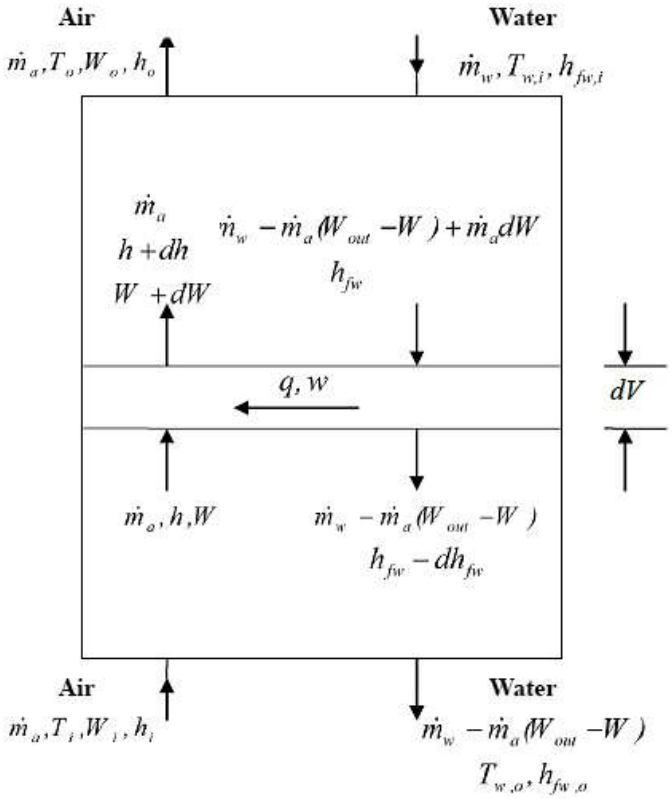

Figure 4. Control volume for conservation of mass and energy balance in a counter flow cooling tower.

$$\frac{dh_{f,w}}{dW} = \frac{1}{\left(\dot{m}_{w,in} - \dot{m}_a(W_{out} - W)\right)}\left[Le_f \frac{(h_{s,w} - h)}{(W_{s,w} - W)} + \left(h_{fg,w} - h_g^0 . Le_f\right) - h_{f,w}\right] \quad (30)$$

For evaluating the temperature distribution, the Equation (31) is used.

$$dT_w = -\frac{1}{c_w}\frac{\left(dh - dW . h_{f,w}\right)}{\frac{\dot{m}_w}{\dot{m}_a} - (W_{out} - W)} \quad (31)$$

In the Equations (28) to (31), the coefficient of mass transfer is unknown. This problem is often resolved using Equation (32).

$$\frac{h_D . A_V . V}{\dot{m}_{w,in}} = c\left(\frac{\dot{m}_{w,in}}{\dot{m}_a}\right)^n \quad (32)$$

In which n and c are the experimental coefficients used for the tower design. Braun has fitted the curve of the cited *n* and *c*. This work has been executed based on Simpson and Sherwood (1946) measurements, for different tower designs operating under design conditions (Braun et al., 1989). The values of *c* and *n* in present model are considered 1.405 and -0.727 respectively based on Braun work.

By multiplying both sides of Equation (32) in ($\dot{m}_{w,in}/\dot{m}_a$) and considering the definition of Number of Transport Units (*NTU*), the experimental value of *NTU* is achieved as Equation (33) represents.

$$NTU = \left.\frac{h_D . A_V . V}{\dot{m}_a}\right|_{em} = c\left(\frac{\dot{m}_{w,in}}{\dot{m}_a}\right)^{n+1} \quad (33)$$

The effectiveness of the cooling tower is defined as the ratio of the actual energy to the maximum possible energy and is calculated using Equation (34).

$$\varepsilon = \frac{h_{out} - h_{in}}{h_{s,w} - h_{in}} \quad (34)$$

Also, it is necessary to define the non-dimensional temperature difference, or temperature ratio in the cooling tower literature, as the ratio of the actual loss to the maximum value through Equation (34).

$$R_{ct} = \frac{T_{w,in} - T_{w,out}}{T_{w,in} - T_{wb,in}} \quad (35)$$

In extracting Equations (14) to (34), it is assumed that there is no resistance against the heat flow in the air-water interface. In other words, the common interface temperature is assumed to be equal to the water bulk temperature. In this way, all of the terms in Equations (14) to (34) which have the subscripts (s, w) are substituted by (s,int). Jabir and Web assumed that T_w is approximately near to T_{int}+*0.5* (Jaber and Webb, 1989).

Figure 5 illustrates both enthalpies of the saturated water-air mixture and the operating line of the tower as a function of water temperature. By assuming a low difference between the values of $h_{s,w}$ and $h_{s,int}$ on the saturated line as a linear function, Equation (36) could be derived.

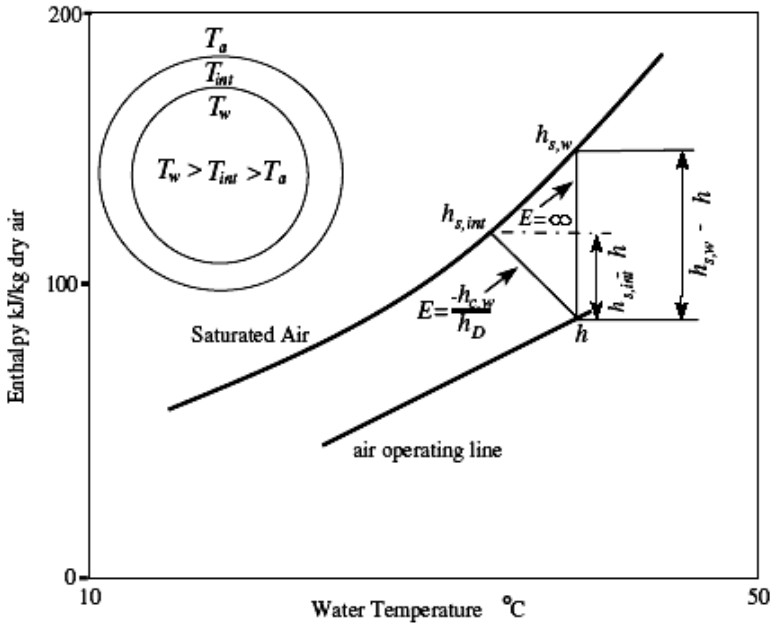

Figure 5. Water operating line on the temperature-enthalpy diagram, indicating the effect of $E = -h_{c,w}/h_D$ on the saturated air enthalpy.

$$h_{s,w} - h = h_{s,w} - h_{s,int} + E(T_w - T_{int}) \quad (36)$$

The slope E is calculated utilizing the Equation (37).

$$E = -\left(\frac{h_{c,w}}{h_D}\right) \quad (37)$$

Equation (37) could be used to determine the temperature at the interface. For large values of *E*, interface and bulk temperatures are approximately equal.

Based on what has been said so far, the term of the average mass transfer coefficient ($h_D A_V$), could be calculated using experimental results of Simpson and Sherwood (1946). In the present paper, besides the experimental exit temperatures, the water mass transfer coefficient, k'_a, and the total heat transfer coefficient, K'_a, have been calculated too. The two aforementioned coefficients could be correlated through Equation (38)

$$\frac{h_{s,w} - h}{h_{s,int} - h} = -\frac{k'_a}{K'_a} \quad (38)$$

By assuming that the interface and bulk temperatures are equal, the last two coefficients also would have the same value. The experimental data will hand in the value of the average mass transfer coefficient, K'_a.

RESULTS AND DISCUSSION

In this work, effects of ambient temperature and relative humidity on the performance and water consumption of a power plant for four mentioned cooling systems are investigated for case study of Hamedan Power plant. Also, cases are economically compared and the best choice is distinguished.

Effect of ambient temperature

The most important parameter that influences performance of cooling towers is the ambient temperature. Changes of ambient temperature cause changes in heat transfer rate of towers. It is clear that the increase of the ambient temperature generally causes an increase in condenser temperature, and, as a result, reduces the output power of the turbine. Furthermore, performance of dry cooling towers is more dependent on ambient temperature in comparison with wet cooling towers, since heat release mechanism in wet cooling towers are mostly through evaporation.

In order to determine the amount of power loss due to changes in ambient temperature for each case in Hamedan power plant, the following steps have been taken. First, the generated power in a 250 MW power plant was computed as a function of ambient temperature based on the equations mentioned in the theory modeling. The range of temperature is considered between 0 and 40°C. Figure 6 illustrated output power of the power plant versus ambient temperature for four cases.

As shown in Figure 6, the augmentation of the ambient temperature leads to the diminution of the plant's power generation, since the first causes the diminution of the dry cooling tower effectiveness and then the augmentation of the exit water temperature. This augmentation in temperature makes the turbine inlet pressure higher and, as a result, lowers its generated power. But as shown in this figure, ambient temperature does not affect

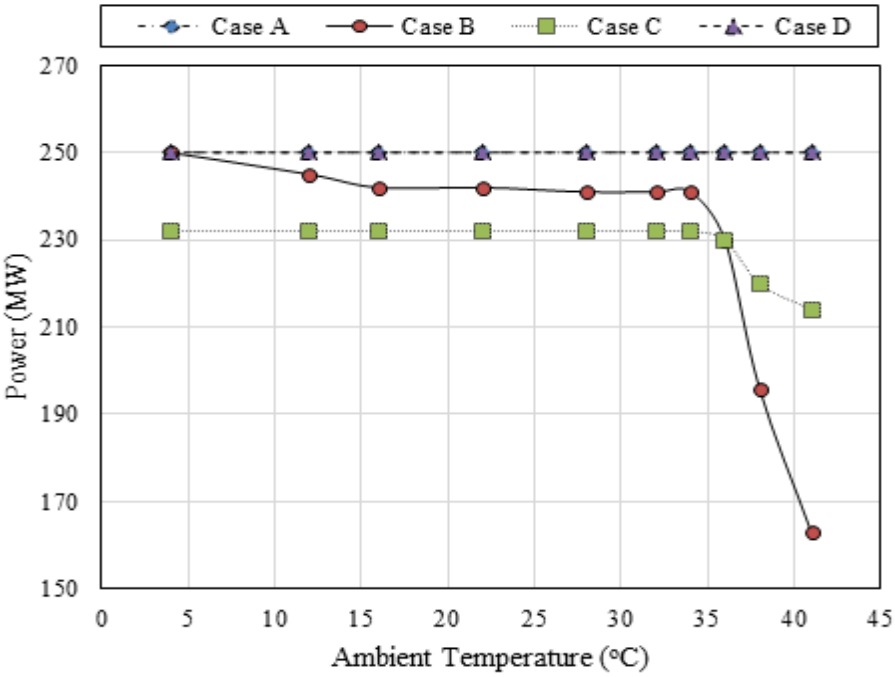

Figure 6. Power generations for mentioned cases as a function of ambient temperature.

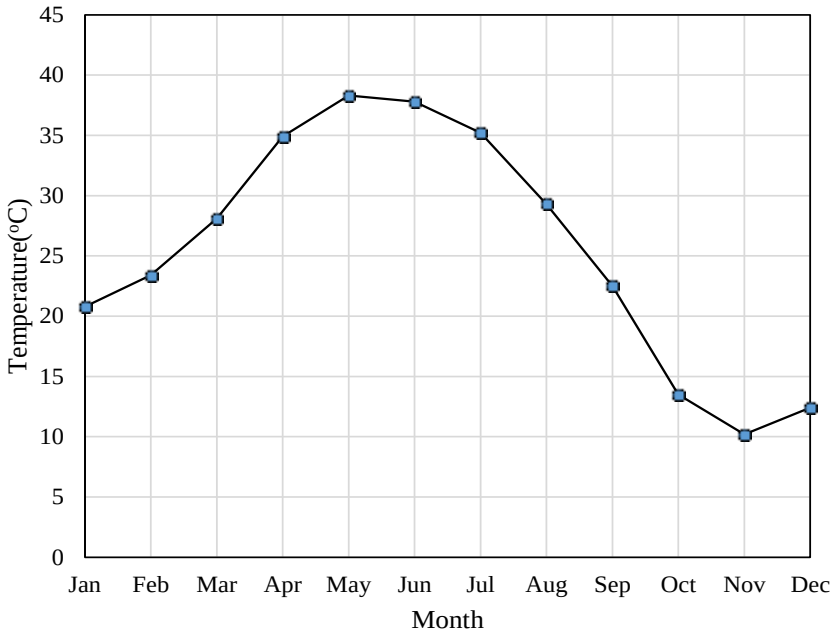

Figure 7. Monthly temperature of Hamedan Power plant.

performance of cases A and D, because of the presence of wet cooling towers.

As mentioned before, case study of current paper is Hamedan Power plant in Iran. So for calculating the amounts of the annual energy loss due to the ambient temperature, diagram of temperature for Hamedan Power plant versus month was collected (Figure 7). Based on Figures 6 and 7, the annual amount of power produced and that of any month can be calculated.

By utilizing Figures 6 and 7, energy production of the power plant for each case versus month can be extracted which is shown in Figure 8. As shown in this figure, there

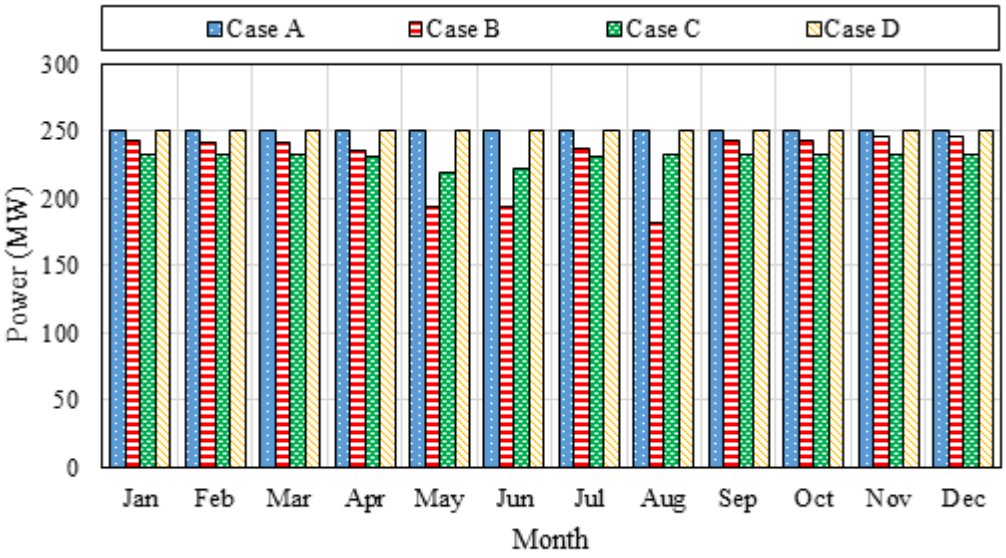

Figure 8. Monthly power production due to the ambient temperature of Hamedan power plant for four mentioned cases.

Table 3. Comparison between energy losses during a year of different methods due to ambient temperatures.

Case	Energy loss during a year (MWh)	Annual investment loss ($)
A	0	0
B	186,624	2,799,360
C	174,240	2,613,600
D	0	0

is no power loss in cases A and D since full capacity of wet cooling towers is achieved and evaporation heat transfer mechanism can supply the amount of heat transfer required for full capacity power generation of the power plant. After these cases, case C has the most power generation due to its utilization of wet cooling towers. Finally, dry cooling towers produce the higher back pressure of turbine that, as a result, has more power loss in comparison with other alternatives.

So the amount of annual power loss due to the ambient temperature is calculated. By utilizing amounts of power generation at each case, as well as regarding the cost of electricity in Iran that is 15$ per MWh, the amount of total annual investment loss can be calculated too. These results are shown in Table 3.

Effect of humidity

In wet cooling towers, by increasing relative humidity, the efficiency of the system decreases due to mechanism of cooling system which is mainly arising from evaporation. So, the more decreases in relative humidity of ambient air, the more capability of evaporation that causes increasing of cooling capacity. But in dry cooling towers, because of the convective heat transfer mechanism, relative humidity does not have noticeable effect and is considered as a second factor (Mehdi, 2000)

In order to determine the power loss in power plants due to changes in relative humidity, first of all, the generated power in a 250 MW power plant was computed as a function of relative humidity due to the relations mentioned in the theory modeling. The range of relative humidity is considered between 0 and 1. Figure 9 illustrated power of power plant versus relative humidity for four cases.

As illustrated in Figure 9, and as mentioned before, relative humidity does not have noticeable effect on performance of dry cooling towers. On the other hand, despite of the presence of wet cooling towers in other alternatives, since present wet cooling towers are including forced-draft fans, lack of heat transfer can be compensated by changing pitch angle of the fans and also more flow rate of the cooling water. So, in these cases power loss is negligible. On the other word, however relative humidity has noticeable effect on

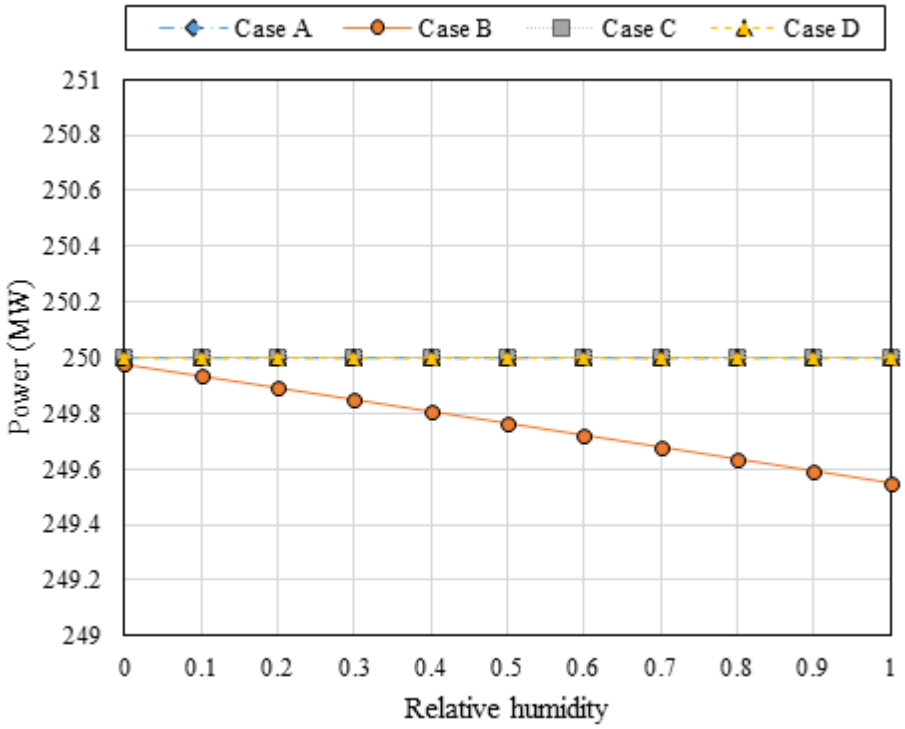

Figure 9. Power generations as a function of relative humidity.

Table 4. Comparison amounts of water consumption between different methods.

Case	Total annual water demand (m^3/y)	Costs of water consumption ($)
A	11,000,000	1,320,000
B	850,000	102,000
C	1,375,000	165,000
D	2,750,000	330,000

performance of wet cooling towers, in present power plant, wet cooling towers have been designed in a way that they can overcome to the relative humidity by increasing flow rate of the cooling water and pitch angle and speed of the fans. This fact was observed directly from data sheets of the power plant during the year. But, as discussed before, by increasing relative humidity more circuit water is needed in order to overcome power loss and this needs more cooling water in hot days of the year. This is going to be considered in estimating the amount of water consumption.

Water consumption

Using thermodynamic analysis for Hamedan power plant in Iran, average annual amounts of water consumption for four alternatives was calculated and is shown in Table 4. Amounts of water consumption are different in four cases due to the structure of cases. It is clear that dry cooling towers have the least amount of water consumption and are suitable for places which confront the problem of water shortage, even though performance and power generation is lower than other cases. Wet cooling towers have the most water demand; but their performance is the most appropriate for regions that have enough sources of water. It was an interesting comparison with combined cooling system cases. In fact, these cooling systems can be utilized in places that have midrange sources of water and also need high performance and power generation. Case D has more annual water demand than case C. Instead, approximately there is no power loss in this case. On the other hand, in comparison with wet cooling towers, it has lower annual water demand and has the same performance, but need more capital cost due to the utilization of dry cooling towers. On the other side, considering that the water price is 0.12$ per cubic meter in industrial

Table 5. Total investment cost amounts of different methods.

Case	Capital cost ($)	Annual running cost ($)
A	38,514,149	3,999,400
B	18,373,851	2,781,400
C	56,888,000	2,844,400
D	56,888,000	3,174,400

applications in Iran, amount of water consumption cost as running cost can be computed for each case that is shown in Table 4.

Economic analysis

Utilizing mentioned descriptions and, also, an exact investigation of required utilities and instruments of each case, amounts of capital and annual running costs of each case was computed. It should be reminded that capital cost of cases C and D are similar due to similarity of structures and just running costs are different.

Cost details of this project consists of the expenditure of purchasing requirement equipment and building structures as capital cost, operating and maintenance costs and water demand as running cost. In addition, power production sales are considered as income of the work. Capital and annual running costs of different alternatives (for building and operating of cooling systems) are listed in Table 5.

In this study, three commonly methods are applied for economic evaluation: Net present value (NPV), internal rate-of-return (IRR) and normal payback method (NP). A brief mathematical model of them will be presented.

The net present value (NPV) method recognizes the surplus of benefits over costs, where all measures are reduced for their time value. (If costs exceed benefits, net damages result). Also, The NPV method is often called the net present worth or net savings method. When this method is applied for measuring a cost-reducing investment, the cost savings are the benefits, and it is often called the net savings (NS) method. NPV from an investment, such as an investment is calculated by following equation:

$$NPV_{A1:A2} = \sum^{N} \frac{B_t - C_t}{(1+d)^t} \quad (39)$$

where $NPV_{A1:A2}$ is NB, for example present value benefits (savings) net of present value costs for alternative *A1* as compared with alternative *A2*, B_t is benefits in year t, which may be specified to contain energy savings, C_t is costs in year *t* related with alternative *A1* as compared with a mutually exclusive alternative *A2*, and *d* is the reduce rate.

The internal rate-of-return (IRR) method solves for the discount rate for which dollar savings are just equal to dollar costs over the analysis duration; that is the rate for which the NPV is zero. This discount rate is the rate of Payback the investment. It is compared to the investor's minimum plausible rate of return to specify whether the investment is favorable. Unlike the preceding three techniques, the internal rate of return does not call for the inclusion of a prespecified discount rate in the calculation; rather, it solves for a discount rate.

The rate of return is usually computed by a process of trial and error, by which diverse compound rates of interest are applied to discount cash flows until a rate is found for which the NPV of the investment is zero. The method has the following procedure: (1) Compute NPV using Eq. (39), except substitute a trial interest rate for the discount rate, *d*, in the equation. A positive NPV means that the IRR is greater than the trial rate; a negative NPV means that the IRR is less than the trial rate. (2) Based on the information, try another rate. (3) By a series of iterations, find the rate at which NPV is zero.

In this study, economic analysis was conducted based on following assumptions in order to render the analysis more traceable:

i) Construction time of the project is considered 2 years.
ii) Operation time of the project is considered 20 years.
iii) Inflation is assumed 15% based on reports of Central Bank of Iran.
iv) Tax is considered to be 5% of the benefits.
v) Load factor is assumed to be 0.65 for all cases.

The above assumptions are based on typical value in Iran. Economic analysis results for different alternatives are listed in Table 6.

As shown in Table 6, the best choice from the economic aspect is case B, that is, utilizing dry cooling towers. On the other hand, negative NPV in case C shows that this case does not have economic justification. But it should be noted that although dry cooling towers have the most economic benefit, they have relatively large power loss, especially in summer times. But, on the other hand, they have the least water consumption among other alternatives. So, it should be considered that based on which one of the following parameters, power production or water consumption, is more important in a specific region, the final decision will be different. As

Table 6. Economic analysis results.

Case	IRR (%)	NPV ($)	NP (year)
A	34.44	24,320,072	3.95
B	48.28	17,516,140	3.71
C	20.09	-22,570,974	5.98
D	21.02	3,431,506	5.78

a matter of fact, if a region is faced with lack of water sources, like case study of current paper, Hamedan Power plant, it is preferable to use dry cooling towers alone. But if national power grid needs full load capacity of the power plant, case D, that is, utilizing combined cooling system that generates full load power, is more suitable. For places near water sources like lakes and rivers, certainly case A, that is, using wet cooling towers, will be the best choice.

Conclusion

The cooling towers are among the most crucial components of every thermal power plant. Their performance directly affects the outlet power and the plant efficiency. Although there have been many works in background of effects of different parameters on performance of cooling towers, there is no detail analysis about different alternatives of hybrid cooling systems due to the water consumption, to the knowledge of the authors. So, in the present work, the effects of the ambient temperature and relative humidity on dry, wet and two cases of combined cooling towers (which designed based on water consumption) performance were studied. Results showed that the plant power generation generally declines with the increase in the ambient temperature and relative humidity, which have matching with pervious works. All of the simulations were executed for a 250 MW plant capacity. Finally, the amount of water consumption of the dry, wet and hybrid towers is evaluated. The results maintained that the need for the make-up water increases as an outcome of augmentation of either ambient temperature or relative humidity. Finally, by an economic analysis, dry cooling system was determined to be the best choice, from both the economical aspect and the amount of water consumption of the case study, Hamedan Power plant in Iran.

Conflict of Interests

The authors have not declared any conflict of interests.

REFERENCES

Al-Waked R, Behnia M (2004). “The performance of natural draft dry cooling towers under crosswind: CFD study. Int. J. Energy Res. 28:147-161.

ASHRAE (1975). ASHRAE Handbook and Product Directory-Equipment, chap. 21, American Society of Heating, Refrigerating and Air Conditioning Engineers, Atlanta GA,USA.

Berman L (1961). Evaporative cooling of circulating water. Pergamon, New York 1961.

Bernier M (1995). Thermal performance of cooling towers. ASHRAE J. 1995.

Braun J, Klein S, Mitchell J (1989). Effictiveness models for cooling towers and cooling coils. ASHRAE Trans. 95(2).

Dachun Y, Chenxin L (1987). Wind tunnel simulation of wind effect on a group of high cooling towers. Acta Mech. Sin. 3(1):36-43.

du Preez AF, Kröger DG (1995). The effect of the heat exchanger arrangement and wind-break walls on the performance of natural draft dry-cooling towers subjected to cross-winds. J. Wind Eng. Ind. Aerodyn. 58(3):293–303.

Harnach R, Niemann HJ (1980). The influence of realistic mean wind loads on the static response and the design of high cooling towers. Eng. Struct. 2:27-34.

He S, Guan Z, Gurgenci H, Hooman K, Lu Y, Alkhedhair AM (2015). Experimental study of the application of two trickle media for inlet air pre-cooling of natural draft dry cooling towers. Energy Convers. Manag. 89:644-654.

He S, Guan Z, Gurgenci H, Jahn I, Lu Y, Alkhedhair AM (2014). Influence of ambient conditions and water flow on the performance of pre-cooled natural draft dry cooling towers. Appl. Therm. Eng. 66(1–2):621–631.

Jaber H, Webb RL (1989). Design of Cooling Towers by the Effectiveness-NTU Method. J. Heat Transf. 111(4):837.

Ke S, Ge Y (2014). “The influence of self-excited forces on wind loads and wind effects for super-large cooling towers.” J. Wind Eng. Ind. 132:125-135.

Kinnon ECP, Golding SD, Boreham CJ, Baublys KA, Esterle JS (2010). “Stable isotope and water quality analysis of coal bed methane production waters and gases from the Bowen Basin, Australia.” Int. J. Coal Geol. 82(3-4):219-231.

Know HowDocuments (1984). Ref. No. 8428 – LK، 1984، EGI، Budapest.

Lucas M, Martínez PJ, Ruiz J, Kaiser AS, Viedma A (2010). “On the influence of psychrometric ambient conditions on cooling tower drift deposition.” Int. J. Heat Mass Transf. 53(4):594-604.

Ma H, Si F, Li L, Yan W, Zhu K (2015). Effects of ambient temperature and crosswind on thermo-flow performance of the tower under energy balance of the indirect dry cooling system. Appl. Therm. Eng. 78:90-100.

Mehdi RL (2000). Conceptual design of main Heller cooling system, “Center of Power Research (MATN)”, Ref. No. ME-04D0-02, 2000, Iran.

Moffat R (1966). The periodic flow cooling tower: a design analysis. Standford Univ. 1966.

Muangnoi T, Asvapoositkul W, Wongwises S (2008). “Effects of inlet relative humidity and inlet temperature on the performance of counterflow wet cooling tower based on exergy analysis.” Energy Convers. Manag. 49(10):2795-2800.

Papaefthimiou VD, Rogdakis ED, Koronaki IP, Zannis TC (2012). Thermodynamic study of the effects of ambient air conditions on the thermal performance characteristics of a closed wet cooling tower. Appl. Therm. Eng. 33–34:199-207.

Sadafi MH, Jahn I, Hooman K (2015b). Cooling performance of solid containing water for spray assisted dry cooling towers. Energy Convers. Manag. 91:158-167.
Sadafi MH, Jahn I, Stilgoe AB, Hooman K (2015a). “A theoretical model with experimental verification for heat and mass transfer of saline water droplets. Int. J. Heat Mass Transf. 81:1-9.
Simpson WM, Sherwood TK (1946). Performance of small mechanical draft cooling towers. Refrig. Eng. 52(6):535-543-576.
Söylemez MS (2004). On the optimum performance of forced draft counter flow cooling towers. Energy Convers. Manag. 45(15-16):2335-2341.
Su MD, Tang GF, Fu S (1999). Numerical simulation of fluid flow and thermal performance of a dry-cooling tower under cross wind condition. J. Wind Eng. Ind. Aerodyn. 79(3):289-306.

Nomenclature

A: Surface area
A_f: The outer surface of the pipe
A_i: Inner surface of the tube
A_t: Average heat transfer area of the tube
A_{fr}: Front surface of the heat exchanger
h: Heat transfer coefficient
h_a: External flow heat transfer coefficient (air side)
h_C: Convective heat transfer coefficient
h_D: Convective mass transfer coefficient
h_W: Internal flow heat transfer coefficient (water side)
K: Thermal conductivity of the pipe
$\dot{m}_a$: Mass flow rate through a column of heat exchanger
$\dot{m}_{a,t}$: Total mass flow rate of air
$\dot{m}_{w,t}$: Total mass flow rate of water
Q_{ow}: Flow rate of water through a column of heat exchanger
$\dot{Q}_C$: Released heat from condenser
R_f: Sediment coefficient
T_{wi}: Inlet water temperature
T_{wo}: Outlet water temperature
U: Total heat transfer coefficient
U_c: Total heat transfer coefficient based on cold surface
W: Absolute humidity

Greek symbols

δ: Thickness of the tube
η: Efficiency of the fin and tube
ρ_{oa}: Air specific mass at standard conditions
ρ_{ma}: Average air specific mass through a heat exchanger.

International Journal of Physical Sciences

academicJournals